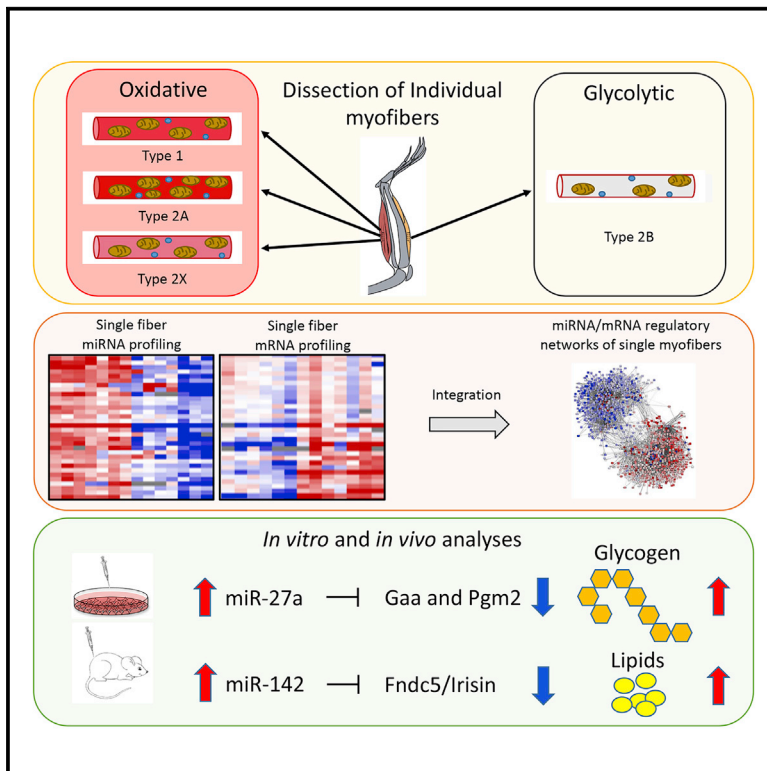


Cell Reports

Transcriptomic Analysis of Single Isolated Myofibers Identifies miR-27a-3p and miR-142-3p as Regulators of Metabolism in Skeletal Muscle

Graphical Abstract



Authors

Francesco Chemello, Francesca Grespi, Alessandra Zulian, ..., Luca Scorrano, Stefano Cagnin, Gerolamo Lanfranchi

Correspondence

stefano.cagnin@unipd.it (S.C.),
gerolamo.lanfranchi@unipd.it (G.L.)

In Brief

Chemello et al. characterize coding mRNAs and non-coding microRNAs expressed by myofibers of hindlimb mouse muscles, identifying complex interactions between these molecules that modulate mitochondrial functions and muscle metabolism. They demonstrate that specific short non-coding RNAs influence the contractile fiber composition of skeletal muscles by modulating muscle metabolism.

Highlights

- Transcriptional networking distinguishes myofibers as glycolytic or oxidative
- miR-27a-3p and miR-142-3p influence mitochondrial morphology
- miR-27a-3p improves lipid use and increases glycogen storage
- miR-142-3p reduces lipid use



Transcriptomic Analysis of Single Isolated Myofibers Identifies miR-27a-3p and miR-142-3p as Regulators of Metabolism in Skeletal Muscle

Francesco Chemello,^{1,2} Francesca Grespi,^{1,3} Alessandra Zulian,⁴ Pasqua Cancellara,⁴ Etienne Hebert-Chatelain,^{1,3} Paolo Martini,¹ Camilla Bean,^{1,3} Enrico Alessio,^{1,2} Lisa Buson,¹ Martina Bazzega,¹ Andrea Armani,³ Marco Sandri,^{3,4,6} Ruggero Ferrazza,⁵ Paolo Laveder,¹ Graziano Guella,⁵ Carlo Reggiani,⁴ Chiara Romualdi,¹ Paolo Bernardi,⁴ Luca Scorrano,^{1,3} Stefano Cagnin,^{1,2,6,*} and Gerolamo Lanfranchi^{1,2,6,7,*}

¹Department of Biology, University of Padova, Via Ugo Bassi 58/b, 35131 Padova, Italy

²CRIBI Biotechnology Centre, University of Padova, Via Ugo Bassi 58/b, 35131 Padova, Italy

³Venetian Institute of Molecular Medicine, Via Orus 2, 35131 Padova, Italy

⁴Department of Biomedical Sciences, University of Padova, Via Ugo Bassi 58/b, 35131 Padova, Italy

⁵Department of Physics, University of Trento, Via Sommarive 14, 38123 Povo (Trento), Italy

⁶CIR-Myo Myology Center, University of Padova, Via Ugo Bassi 58/b, 35131 Padova, Italy

⁷Lead Contact

*Correspondence: stefano.cagnin@unipd.it (S.C.), gerolamo.lanfranchi@unipd.it (G.L.)

<https://doi.org/10.1016/j.celrep.2019.02.105>

SUMMARY

Skeletal muscle is composed of different myofiber types that preferentially use glucose or lipids for ATP production. How fuel preference is regulated in these post-mitotic cells is largely unknown, making this issue a key question in the fields of muscle and whole-body metabolism. Here, we show that micro-RNAs (miRNAs) play a role in defining myofiber metabolic profiles. mRNA and miRNA signatures of all myofiber types obtained at the single-cell level unveiled fiber-specific regulatory networks and identified two master miRNAs that coordinately control myofiber fuel preference and mitochondrial morphology. Our work provides a complete and integrated mouse myofiber type-specific catalog of gene and miRNA expression and establishes miR-27a-3p and miR-142-3p as regulators of lipid use in skeletal muscle.

INTRODUCTION

Half of the body mass of healthy individuals is composed of skeletal muscle that supports body movements and is crucial for intermediate metabolism. As a metabolic organ, skeletal muscle regulates systemic glucose homeostasis. When glucose is not consumed as fuel, it accumulates as glycogen in muscle, and this storage can be almost 5 times more efficient as in the liver (Jensen et al., 2011). However, during physiological changes such as fasting, muscle can rapidly adapt to use fatty acids (FAs) and amino acids as oxidative substrates. Not surprisingly, impairment in muscle metabolic plasticity and insulin sensitivity is a hallmark of several metabolic diseases, including type 2 diabetes and obesity (Sears and Perry, 2015).

Skeletal muscle retains remarkable metabolic malleability despite the fact that its anatomical units are terminally differen-

tiated, post-mitotic cells. In this situation, the adaptive capacity must rely on complex but ordered changes in the pattern of gene expression in the fiber nuclei (plus post-translation protein modifications), responding to specific physiological stimuli. Many studies have demonstrated modifications in the gene expression profile of muscles with different metabolic traits (Campbell et al., 2001; Wu et al., 2003) and the presence of sensor molecules that, upon specific stimulation, may act as modifier of gene transcription (Bean et al., 2008; Carrasco and Hidalgo, 2006; de Lange et al., 2007; Egan and Zierath, 2013). The flexibility of skeletal muscle in the use of carbohydrates or lipids is associated with the expression of different panels of structural proteins that ultimately define different contractile properties (Schiaffino and Reggiani, 2011). The overall physiological diversity and plasticity is based on the repertoire and proportion of different types of myofibers that compose a particular muscle in a particular physiological condition. In small mammals, slow muscles such as soleus are composed mostly of slow-oxidative myofibers that express the slow type 1 myosin heavy chain (MyHC) and fast-oxidative myofibers that express type 2A or 2X MyHC. Types 1, 2A, and 2X mouse myofibers are considered oxidative myofibers and largely use lipids to meet the bulk of their energy requirements aerobically. In contrast, fast muscles such as extensor digitorum longus (EDL), gastrocnemius, and tibialis anterior, are composed mostly of fast-glycolytic myofibers that express a predominance of type 2B MyHC and use glucose to produce most energy anaerobically. In addition to the four major types of myofibers, minor intermediate hybrid fibers expressing different combinations of MyHC isoforms can be found in different muscles.

Metabolic adaptation can also occur through the modulation of mitochondrial dynamics (Liesa and Shirihai, 2013; Schrepfer and Scorrano, 2016). In skeletal muscle, mitochondrial dynamics vary in the different myofiber types: mitochondria are elongated because of increased fusion in oxidative myofibers compared with glycolytic myofibers (Mishra et al., 2015).



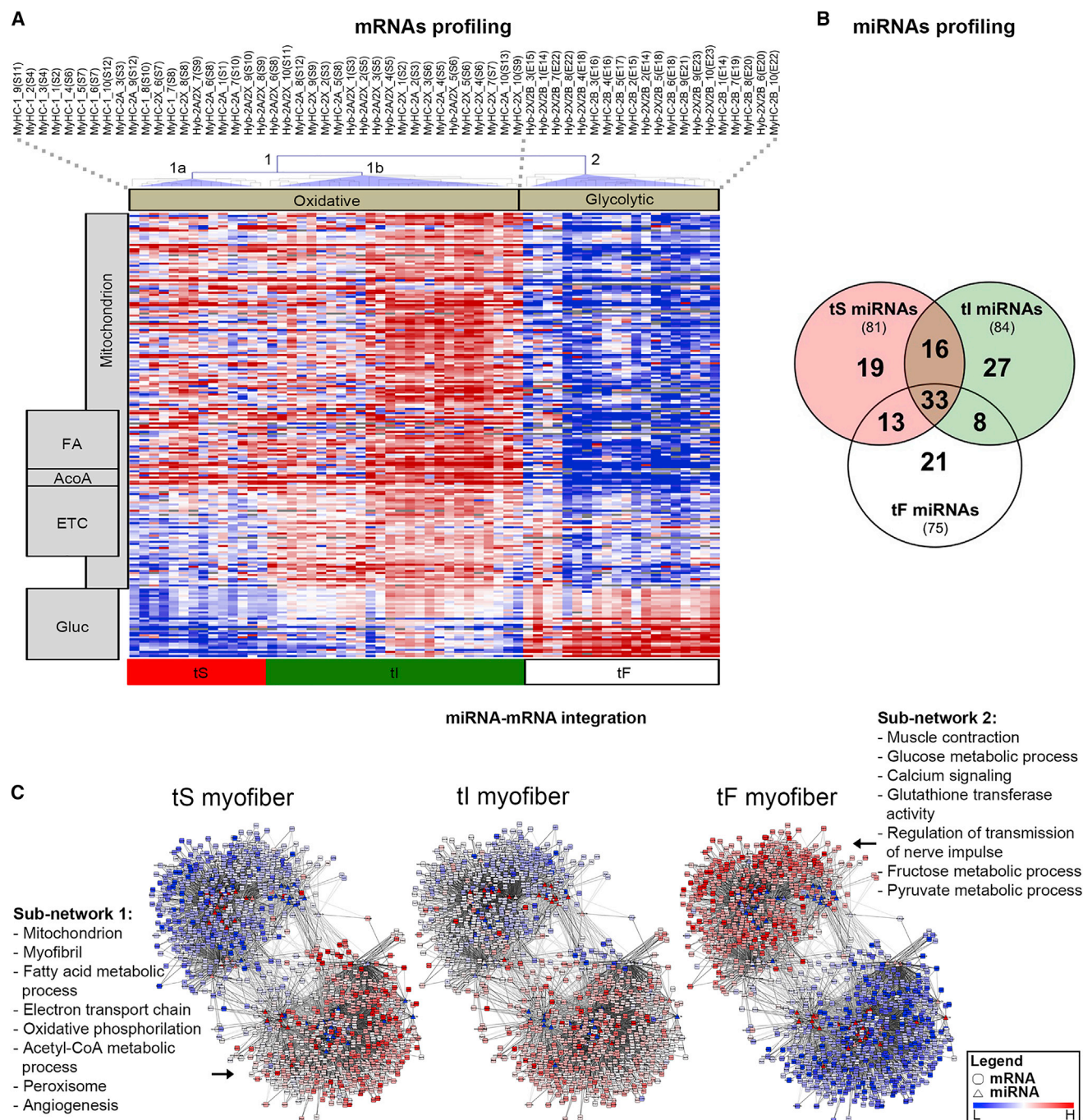


Figure 1. Transcriptional Signatures of Myofibers from Mouse Soleus and EDL

(A) Cluster analysis of the DE microarray probes identifies two main signatures (1 and 2) that reflect fiber metabolism (oxidative and glycolytic, tF). Oxidative signature 1 is further divided in two groups (1a and 1b), which we named transcriptional slow (tS) and transcriptional intermediate (tI). MyHC isoform composition was indicated for pure (MyHC) or hybrid (Hyb) types. Myofibers of the same type were numbered from 1 to 10 and marked with the muscle of origin (S, soleus; E, EDL) and the different mice from which they were isolated (in parentheses). Myofibers were purified from 13 different soleus muscles derived from 13 mice and 10 different EDL muscles derived from 10 mice. The heatmap shows the expression of DE genes involved in metabolism as identified by Gene Ontology (GO) analysis (Table 1) (blue, low expression; red, high expression; gray, under the detection limit). On the left, gene functions are indicated: FA metabolic process (FA), acetyl-CoA metabolic process (AcoA), electron transport chain (ETC), and glucose metabolism (Gluc).

(legend continued on next page)

MicroRNAs (miRNAs) are small non-coding RNAs (20–22 nt long) that post-transcriptionally control gene expression and are thought to play an important role in rapid adaptive metabolic responses (Shimoni et al., 2007). miRNAs were also recently implicated in the regulation of mitochondrial metabolism in skeletal muscle, as mice lacking miR-378-3p and miR-378-5p are resistant to obesity induced by high-fat diet (HFD) and can efficiently oxidize FAs (Carrer et al., 2012).

Here, we compiled a comprehensive catalog of mRNAs and miRNAs expressed in single myofiber types of mouse muscles to avoid the averaging effect of multiple fiber types and signals from non-muscle cells (Chemello et al., 2011, 2015; Mammucari et al., 2015; Murgia et al., 2015). We connected these catalogs to obtain the RNA regulatory networks dictating the metabolic phenotypes of myofibers. Network analysis confirmed that miRNAs interact with nuclear receptors involved in energy homeostasis (Lee et al., 2011) and allowed us to define, both *in vitro* and *in vivo*, the influence of specific miRNAs on mitochondrial shape and respiration, lipid and glycogen use, and oxidative and glycolytic myofiber traits.

RESULTS

The Transcriptional Signature of a Myofiber Echoes Its Metabolic Traits

We undertook a large-scale expression profiling of single isolated myofibers by collecting 100 myofibers from mouse soleus and 100 myofibers from mouse EDL. In a fragment of each fiber, we measured MyHC isoforms as a reference to the canonical fiber catalog (Figure S1A). As expected, this method identified six major patterns of MyHC isoforms, namely 1, 2A, 2A*2X, and 2X for soleus and 2X/2B and 2B for EDL (Table S1). We profiled 10 myofibers from each of the six major MyHC groups (Data S1), generating a collection of 60 transcriptional profiles. Myofibers were purified from 23 different mice. In total, 1,936 probes were differentially expressed (DE) among the fiber repertoire (Data S1). Cluster analysis separated the 60 profiles into a large cluster composed of 40 fibers and a smaller cluster composed of the remaining 20 fibers (Figure 1A). The larger signature was clearly divided in two sub-groups. One, which we named transcriptional slow (tS), was composed mainly of type 1 fibers, and the other, called transcriptional intermediate (tI), was composed of types 2A, 2A-2X, and 2X fibers. The smaller signature, composed of types 2B and 2X/2B fibers, was named transcriptional fast (tF). To obtain a quick and univocal assay for the assignment of myofibers to one of the three signatures, we identified the five genes with the best classification power (Figure S1B) and added to these *Myh2* because (1) it is the best positive marker for the tI signature (Figure S1C; Data S2), and (2) its translated protein (MyHC-2X) is commonly used as a marker for myofiber protein classification. Consistent with this,

our data indicate that the transcriptional levels of *Myh* mRNAs are excellent markers for myofiber typing (Figure S1D).

To understand the functional meaning of the gene-clustering architecture, the DE probes were statistically divided into eight groups according to their expression patterns among myofiber transcriptional types. In addition to the *Myh* family, genes coding for protein isoforms involved in the different speed of contraction of myofibers were separated in the different clusters (i.e., slow isoforms of troponins and tropomyosins were more expressed in tS myofibers, whereas fast isoforms were more abundant in tI and tF myofibers) (Figure S1E; Data S3). Moreover, transcription factors responsible for myofiber contractile and metabolic properties were identified, as a result of the high-resolution power of the single-fiber approach. For example, the slow-myofiber gene repressor *Sox6* (Quiat et al., 2011) is expressed more in tF myofibers, whereas the PPAR (*Ppara*, *Pparg*, and *Ppargc1b*) and ERR (*Esrrb* and *Esrrg*) regulators of oxidative metabolism (Fan and Evans, 2015) are more highly expressed in tS and tI myofibers.

The main biological processes differing among the three myofiber signatures were related principally to cellular metabolism (Table 1; Data S3). Consistent with this, the two major clusters of fiber profiles reflected the two metabolic traits of skeletal muscle tissue (i.e., oxidative and glycolytic). tS and tI myofibers were enriched in genes coding for enzymes involved in FA, electron transport chain, and acetyl-CoA metabolic processes, while tF myofibers preferentially expressed genes coding for proteins involved in glucose metabolism (Figure 1A). These experiments confirmed that different myofiber types display specific metabolic gene signatures. Interestingly, Gene Ontology analysis indicated that mitochondrial genes are particularly upregulated in tI myofibers, suggesting the critical importance of this organelle in the metabolism of this type of myofiber.

miRNAs Post-transcriptionally Regulate Myofiber Metabolism

miRNAs are important post-transcriptional regulators of cell metabolic pathways (Dumortier et al., 2013; Rottiers and Nääär, 2012). To fully explore their role, miRNA and mRNA populations were purified from single isolated myofibers, and miRNA fractions were analyzed using next-generation sequencing (NGS) in each fiber type, after classification using the previously established mRNA markers (Figure S2A). We identified 81 miRNAs expressed in tS, 84 in tI, and 75 in tF myofibers (Figure 1B; Data S4). We recognized 15 significantly enriched families. Among them, 3 belong to known muscle-specific miRNAs (myomiRs) (McCarthy, 2011), namely, miR-1a, miR-1b or miR-206 or miR-613, miR-133a, miR-133b, miR-133c, and miR-486-5p or miR-3107 (Data S4). In addition to miR-1a-3p and miR-133a-3p, which we confirmed as two of the most expressed miRNAs in muscle fibers, we identified

(B) One hundred thirty-seven miRNAs expressed in at least one myofiber transcriptional type were identified: 81 miRNAs were more highly expressed in tS myofibers, 84 in tI myofibers, and 75 in tF myofibers. Thirty-three miRNAs (including the myomiRs miR-1a-3p and miR-133a-3p) are generally expressed across all myofibers. Myofibers were derived from three different soleus muscles and three different EDL muscles (three mice).

(C) Networks describing post-transcriptional regulation in tS, tI, and tF myofibers. Triangles, miRNAs; squares, mRNAs; colors reflect their expression levels. GO enrichment analysis was performed on genes of the two sub-networks (enhanced by the dotted line). Only terms with enrichment scores > 1.3 are listed (the highest at the top).

Table 1. Gene Ontology Analysis of Genes Differentially Expressed among Transcriptional Myofiber Types

	Enrichment Score	p Value
Probes Overexpressed in tS Myofibers (Cluster 1, 114 Probes, 94 DAVID IDs)		
Muscle tissue development	2.14	3.03E−04
Cytoskeletal protein binding	1.96	4.57E−04
Probes Overexpressed in tS and tI Myofibers (Clusters 2 and 3, 806 Probes, 643 DAVID IDs)		
Mitochondrion	23.80	9.37E−33
Fatty acid metabolic process	8.51	6.12E−12
Myofibril	8.18	6.95E−10
Electron transport chain	4.65	5.71E−06
Acetyl-CoA metabolic process	3.52	1.87E−07
Probes Overexpressed in tI Myofibers (Cluster 4, 95 Probes, 85 DAVID IDs)		
Mitochondrion	7.95	2.40E−18
Electron transport chain	5.63	4.12E−13
Probes Overexpressed in tI and tF Myofibers (Cluster 5, 240 Probes, 123 DAVID IDs)		
Glucose metabolic process	9.23	6.64E−10
Muscle contraction	2.40	2.57E−03
Myofibril	1.98	8.80E−04
Probes Overexpressed in tF Myofibers (Clusters 6 and 7, 638 Probes, 506 DAVID IDs)		
Sarcoplasmic reticulum	8.06	8.06E−11
Myofibril	5.61	6.27E−07
Glutathione transferase activity	3.16	2.13E−03
Glucose metabolic process	2.90	1.59E−05
Muscle contraction	2.79	3.73E−04
Gene Ontology (GO) enrichment analysis of the 1,936 DE microarray probes was separately performed on genes that share common expression patterns among the three transcriptional myofiber signatures (tS, tI, and tF; described in Data S3 using the DAVID bioinformatic tool). One representative GO term from each functional annotation cluster with an enrichment score cutoff > 1.3 (the higher, the better) and p values < 0.05 (the lower, the better) was listed. Overlapping functional terms were ignored, and only groups from the top five clusters are shown (additional information is provided in Data S3).		

10 other miRNAs highly expressed in all fiber types ([Table S2](#)). These include almost all members of the let-7 family, indicating their importance in skeletal muscle biology. Interestingly, we could associate specific miRNAs with different transcriptional signatures ([Figure S2B](#)). For example, myomiR-206-3p and miR-208b-3p control skeletal muscle oxidative metabolism ([Boettger et al., 2014; Gan et al., 2013](#)) and are expressed strictly in tS myofibers. In contrast, miR-154 and miR-186, expressed only in tF myofibers, are regulated by glucose concentration ([Jiang et al., 2018; Sun et al., 2014; Wang et al., 2008](#)). qRT-PCR measures of 55 miRNAs confirmed the NGS results with a correlation of 0.78 ([Figure S2C; Data S4](#)). Certain miRNA-3p-miRNA-5p couples were DE across different myofibers, as found in other tissue types ([Martini et al., 2014](#)).

The identification of miRNA targets in a mRNA population is critical. For this reason, putative miRNA targets were extracted from the repertoire of mRNAs expressed in muscle fibers by predictive algorithms and filtered for biological significance. Because miRNAs act through target degradation ([Hu and Collier, 2012](#)), only miRNA-mRNA groups that showed negative correlations between their expression levels were selected for the construction of an integrated network. A total of 5,968 interactions were computed, resulting from the negative correlations between the expression of 79 miRNAs and 1,051 putative mRNA targets ([Data S5](#)). The topology of the miRNA-mRNA interactions clearly draws two sub-networks where miRNAs are placed as central regulators ([Figure 1C](#)). Sub-network 1 is characterized by genes coding for mitochondrial proteins and enzymes involved in oxidative phosphorylation and FA metabolism, whereas sub-network 2 contains genes encoding glycolytic enzymes. Considering the number of edges for each node in the network, it follows that each miRNA, on average, contacts 81 mRNAs, supporting the idea that a single miRNA may regulate many mRNAs. Comparing the networks for tS and tF myofibers, an opposite expression trend is observed for connected genes and miRNAs ([Figure 1C](#)). In tS fibers, transcripts involved in glycolytic metabolism were generally under-expressed, while the connected miRNAs were upregulated. Conversely, transcripts involved in oxidative phosphorylation and FA metabolism were upregulated, while the connected miRNAs were downregulated. On the contrary, tF fibers show opposite expression levels. The network for tI fibers generally showed intermediate expression levels. In summary, this set of data provides a complete cell-specific expression network that may control glycolytic and oxidative metabolic traits in skeletal muscle.

miR-27a-3p and miR-142-3p Influence Mitochondrial Shape and Respiration In Vitro

Because of the large number of DE miRNAs, we selected for functional analyses a set of miRNAs that were connected, in the metabolic networks of [Figure 1C](#), to a different number of transcripts with peculiar expression in myofibers. These are miR-27a-3p and miR-23a-3p, which connected to 114 and 105 putative mRNA targets (higher connections than the mean), grouped in the slow-intermediate expression cluster, and miR-130a-3p and miR-142-3p, which connected to 73 and 48 mRNA targets (lower connections than the mean), included in the slow-intermediate and fast-slow expression clusters. Moreover, for the selection of miRNAs, we also considered their connections with transcripts encoding important proteins involved in metabolic regulation. In whole-muscle analysis, all of these miRNAs are more expressed in the oxidative soleus muscle, confirming single-myofiber results, except for miR-142-3p, which did not vary between fast and slow muscles ([Figure 2A](#)). miR-142-3p was discovered only because of the single-fiber approach and is particularly interesting in terms of its differential expression among myofibers. NGS analysis of single myofibers confirmed that miR-23a-3p, miR-27a-3p, and miR-130a-3p were upregulated in oxidative myofibers, while miR-142-3p was downregulated in tI myofibers ([Figure 2B](#)). Because function and shape of mitochondria

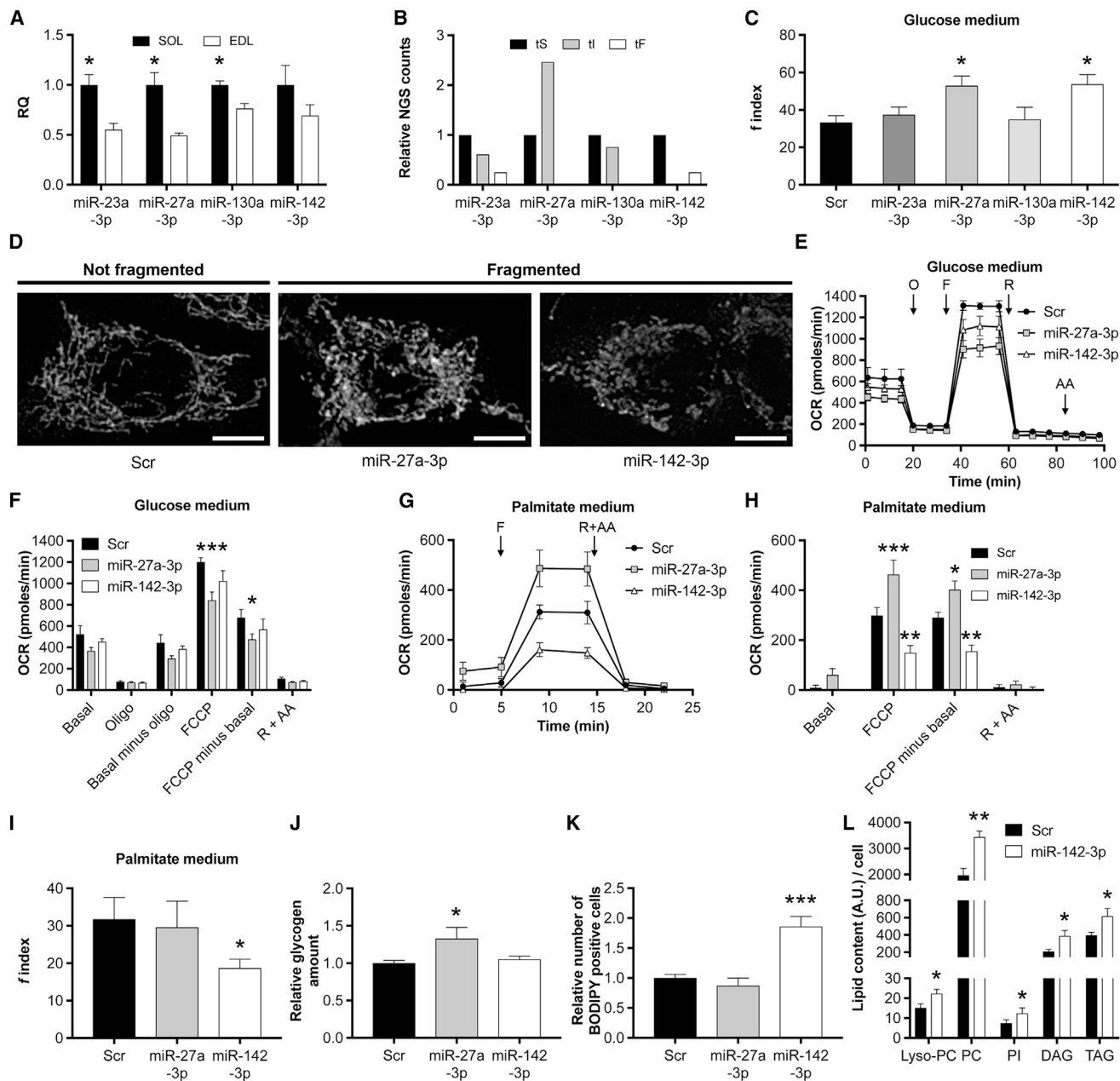


Figure 2. Effects of miR-27a-3p and miR-142-3p on Mitochondrial Morphology and Energy Metabolism: In Vitro Studies

(A) Relative quantification (RQ) by qRT-PCR of the selected miRNAs. miRNA expression levels were tested in slow muscles (soleus [SOL]) and in fast muscles (EDL, used for data normalization). Each experiment was performed with three muscles from different mice in three technical replicates.

(B) NGS results for the selected miRNAs on tS, tI, and tF myofibers. Expression levels were normalized on tS myofibers.

(C) Quantification of the fragmentation index, *f*, of mitochondrial networks after miRNA transfections; *n* = at least 20 for each condition (three independent transfections per mimic).

(D) Representative fluorescence microscopy images of single cells with different levels of mitochondria fragmentation. Mitochondria were stained with anti-TOM20 and imaged using confocal microscopy. Images of each cell were captured at different focal depths and then processed by focal-plane merging and convolution. Scale bar is 10 μ m.

(E and G) Bioenergetic profiles of transfected myoblasts in glucose (E) or palmitate (G) substrate medium. The OCR of C2C12 myoblasts transfected with miRNA mimics was evaluated using the sensitive Seahorse technology after 72 h of transfection. Bioenergetic profiles of cells were measured in a basal state and after the addition of oligomycin (O; to inhibit ATP synthase), FCCP (F; to uncouple ATP synthesis from the electron transport chain), and rotenone and antimycin A (R and AA; to block complexes I and III, respectively, of the electron transport chain). In palmitate medium, lipid-specific respiration was analyzed by acute Cpt1 inhibition by etomoxir. miRNA transfections were independently replicated at least three times, and for each one, five technical replicates were measured.

(F and H) Parameters of mitochondrial function of transfected myoblasts in glucose (F) or palmitate (H) resulting from the bioenergetic profiles.

(legend continued on next page)

are strictly related (Schrepfer and Scorrano, 2016), we examined the role of the four selected miRNAs in mitochondrial morphology. In mouse muscle C2C12 cells, the modification of miR-23a-3p or miR-130a-3p expression did not affect mitochondrial shape, while increased levels of miR-27a-3p or miR-142-3p caused mitochondrial fragmentation (Figures 2C and 2D). Electron microscopy confirmed that myoblasts transfected with these two miRNAs possess smaller and less connected mitochondria, although with quite normal cristae structure (Figure S3A). The altered mitochondrial morphology was accompanied by changes in mitochondrial fuel oxidation. In myoblasts relying on glucose as oxidable substrate, miR-27a-3p caused a significant decrease in maximal oxygen consumption rate (OCR) induced by FCCP (Figures 2E and 2F). When the oxidable substrate was palmitate, miR-142-3p led to decreased, whereas miR-27a-3p increased cellular respiration (Figures 2G and 2H). No alterations in cristae structure were observed in myoblasts overexpressing miR-27a-3p (Figures S3A and S3B). In contrast, myoblasts overexpressing miR-142-3p appeared elongated in palmitate medium (Figure 2I) and presented with a number of vesicles comparable with lipid droplets in the cytoplasm (Figure S3A). We investigated if the alteration of bioenergetics supply, observed in myoblasts transfected *in vitro* with miR-27a-3p or miR-142-3p, could result in accumulation of unused nutrients. Indeed, miR-27a-3p induced the accumulation of glycogen (Figure 2J), whereas miR-142-3p induced the accumulation of lipid droplets in C2C12 myoblasts (Figure 2K), in the proximity of mitochondria (Figure S3C). The overexpression of miR-27a-3p or miR-142-3p also induced the accumulation of glycogen or lipids in primary human myoblasts, indicating that the action of these miRNAs may be shared among other vertebrates (Figures S4A and S4B). Lipidomics analysis of C2C12 myoblasts transfected with miR-142-3p identified 66 lipids, belonging to ten different classes (Data S6), and confirmed an overall increase in lipid content after miR-142-3p overexpression (Figures S3D and S3E for the classes not significantly altered). Phosphatidylcholine (the major phospholipid populating the surface of lipid droplets) and triacylglycerol (the main constituent of the neutral lipid core of lipid droplets) are among the classes of lipids that increased (Figure 2L) and likely constitute the major components of miR-142-3p-induced fat droplets.

These results indicate that miR-27a-3p and miR-142-3p act on cellular metabolic pathways, inducing morphological and physiological dysfunction of mitochondria. FA use is inhibited by

miR-142-3p, and it is improved by miR-27a-3p, whereas glycogen consumption is limited by overexpression of miR-27a-3p. Gene expression analyses of myoblasts overexpressing miR-27a-3p or miR-142-3p were consistent with these functional changes. In fact, miR-27a-3p depressed electron transport chain genes, whereas miR-142-3p turned off genes coding for enzymes involved in FA metabolism (Data S6).

miR-27a-3p and miR-142-3p Influence Metabolism of Muscle Cells by Targeting Pgm2, Gaa, and Fndc5

We next evaluated if miR-27a-3p and miR-142-3p downregulated the putative targets identified by the mRNA-miRNA networks (Figure 1C). Microarray analysis showed that 66.7% and 73.9% of miR-27a-3p or miR-142-3p targets were indeed downregulated (Figure 3A). Because miR-27a-3p influences glycogen use, we searched for genes involved in glycogenolysis in the list of putative targets downregulated in C2C12 cells following overexpression of miR-27a-3p. Phosphoglucomutase (Pgm2) and acid α -glucosidase (Gaa), genes encoding for key enzymes in cytosolic and lysosomal glycogenolysis, were among the targets. The interaction between miR-27a-3p and the 3'-UTR of Pgm2 and Gaa was confirmed by luciferase assay (Figure 3B). In addition, glycogen phosphorylase (Pygm), another important gene for glycogenolysis not directly targeted by miR-27a-3p, was under-represented when miR-27a-3p was upregulated in C2C12 cells (Table S3).

In C2C12 myoblasts overexpressing miR-142-3p, fibronectin type III domain containing 5 (Fndc5), encoding for the precursor of the myokine Irisin (Boström et al., 2012), was the most downregulated gene. A luciferase assay showed a 40% reduction of Fndc5 transcript upon overexpression of miR-142-3p in C2C12 cells (Figure 3B). Transcriptomic analysis of myoblasts overexpressing miR-142-3p indicated that several genes involved in FA metabolism were deregulated. Acyl-CoA synthase 1 (Acsl1), the most important isoform for the synthesis of acyl-CoA used by skeletal muscle mitochondria (Li et al., 2015), was upregulated, confirming an increase in FA anabolism, though other acyl-CoA synthase isoforms (Acsl3 and Acsl6) were downregulated. Genes of FA catabolic enzymes, such as acyl-CoA dehydrogenase (Acad10 and Acad12), or related to FA catabolism, such as carnitine palmitoyl transferase (Cpt2), hormone-sensitive lipase (HSL), and Ucp2 and Ucp3, were downregulated. Conversely, the lipid droplet markers perilipins (Plin1, Plin2, and Plin4) were upregulated (Table S3). The depressive effects of miR-27a-3p and miR-142-3p on mRNA targets is accompanied by the reduction of the encoded

(I) Quantification of the fragmentation index, *f*, of mitochondrial networks after miR-27a-3p or miR-142-3p transfections in palmitate medium. Control experiments performed with BSA alone (necessary for conjugate palmitate; data not shown). For each experiment, *n* = at least 20 (three independent transfections per mimic).

(J) C2C12 myoblasts were transfected with a scramble sequence as control, with miR-27a-3p, or with miR-142-3p. Cells were lysed, and glycogen content was quantified using a luminometer. Data are the mean of two replicates for three independent transfection experiments (*n* = 6).

(K) Transfected myoblasts were stained for lipids with BODIPY fluorophore, and fluorescence-positive cells were counted using flow cytometry. Data are the mean of two replicates for three independent transfection experiments (*n* = 6).

(L) Lipids were extracted from myoblasts transfected with a control scramble sequence or with miR-142-3p and measured with liquid chromatography-mass spectrometry (LC-MS) technology. Classes of lipids significantly different between samples are represented in the figure (DAG, diacylglycerol; Lyso-PC, lyso-phosphatidylcholine; PC, phosphatidylcholine; PI, phosphatidylinositol; TAG, triacylglycerol). Lipid quantification was measured as a.u. of signal areas of chromatograms and normalized to the number of cells relative to each sample. Number of independent experiments (*n*) per condition = 4.

Scr, control transfected with a scrambled sequence. Error bars indicate SEM. Adjusted *p* values from ANOVA (in comparison with control) are indicated as follows: **p* < 0.05, ***p* < 0.01, and ****p* < 0.001.

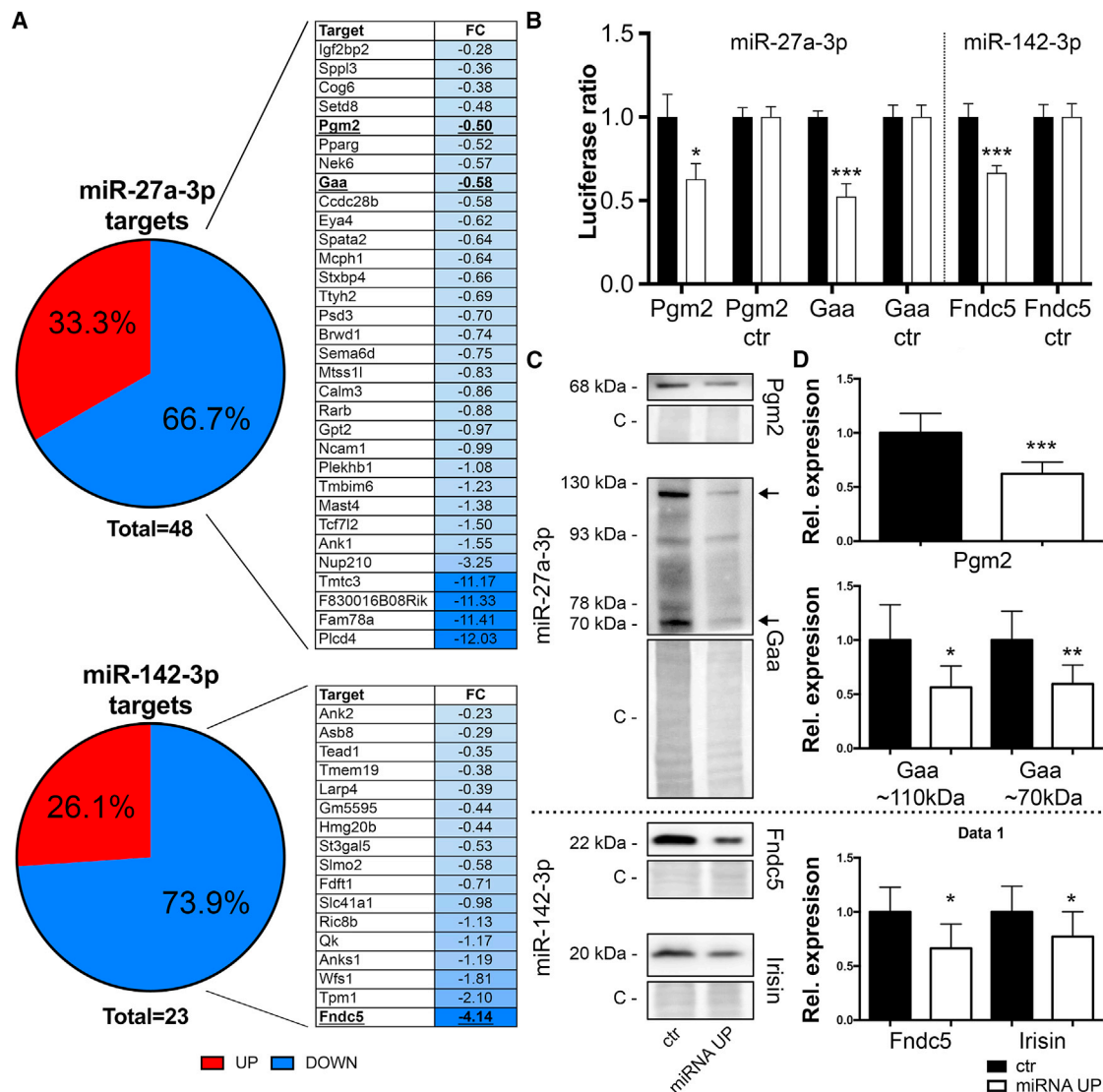


Figure 3. Identification and Characterization of Transcripts that Are Altered by miR-27a-3p and miR-142-3p Overexpression

(A) Expression profiling of myoblasts transfected with miR-27a-3p or miR-142-3p showed that most targets identified in myofiber mRNA-miRNA interaction networks in Figure 1C are downregulated. Thirty-two transcripts of 48 targets of miR-27a-3p (66.7%) are downregulated in C2C12 myoblasts upon overexpression of that miRNA. Similarly, overexpression of miR-142-3p resulted in the downregulation of 17 of 23 targets (73.9%). Tables flanking pie graphs list the expression values (\log_2 fold change [FC]) of downregulated miRNA targets in transfected myoblasts in comparison with myoblasts transfected with a scrambled sequence as control (Scr). Data are the mean of six independent transfections for each miRNA mimic and four independent transfections for Scr.

(B) Luciferase assays were performed to demonstrate the direct interaction between the two miRNAs and their targets. Part of the 3'-UTR sequence containing the miRNA putative interaction site (or not containing; ctr) was cloned in pmirGLO vector. Firefly luciferase (reporter gene) and Renilla luciferase (control reporter for normalization) activities were measured after the transfection in C2C12 cells together with miRNA mimics or miRNA Scr sequence. Data are expressed as the mean of at least five independent transfections. Error bars indicate SEM. p values from t tests are indicated as follows: *p < 0.05 and ***p < 0.001.

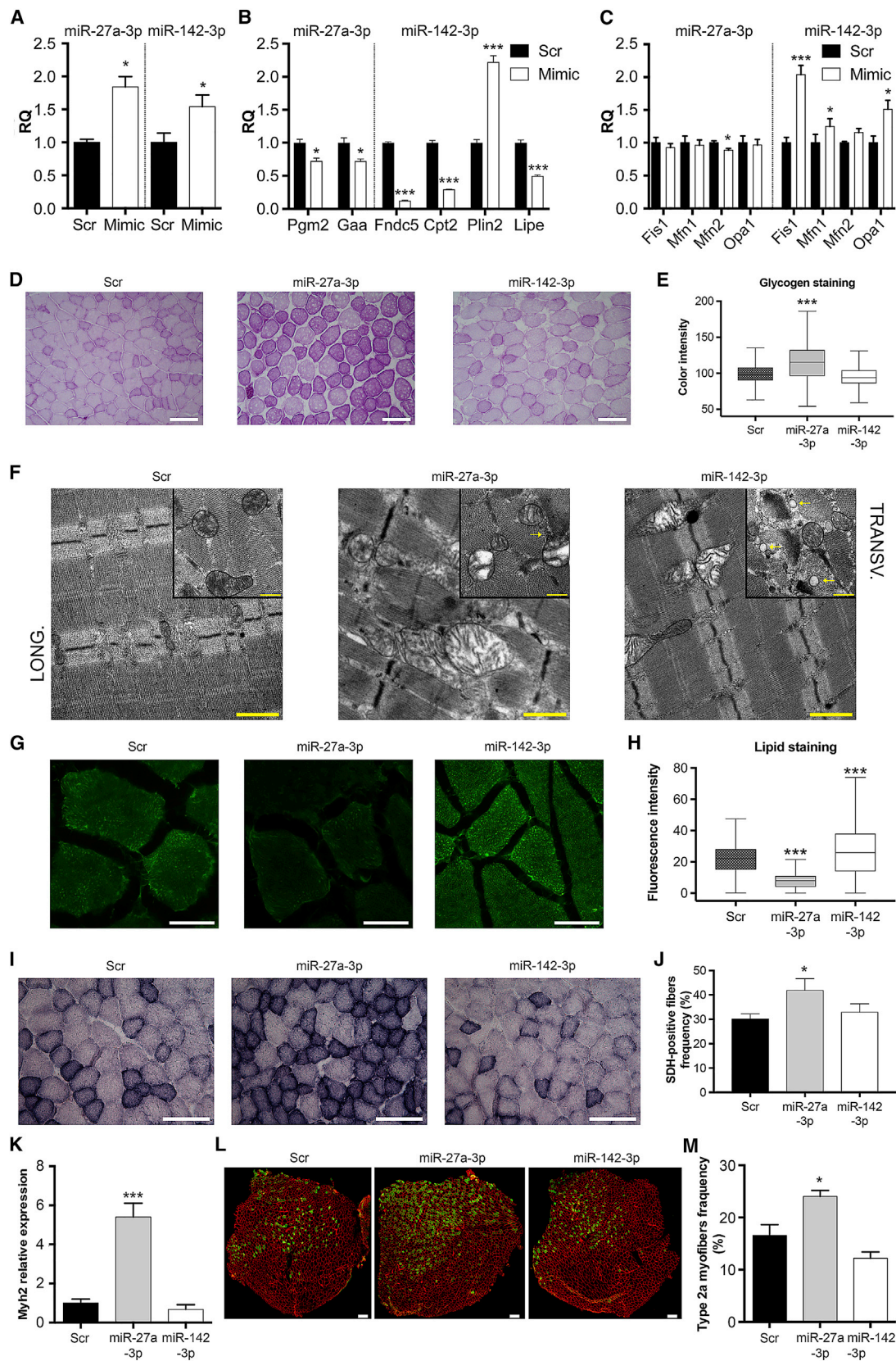
(C) Western blots of miRNA target proteins of C2C12 myotubes in which either miR-27a-3p or miR-142-3p was overexpressed. Both immunoreactive bands (top) and the corresponding Coomassie blue staining (C; bottom) are shown. Arrows indicate the Gaa isoforms of 70 and 110 kDa.

(D) Densitometric analysis of western blots in which the optical density of immunoreactive bands was normalized to the optical density of the corresponding Coomassie-stained lane. Data are expressed as mean of at least four independent transfections. Error bars are SEM. p values from t tests are indicated as follows: *p < 0.05, **p < 0.005, and ***p < 0.001.

proteins Pgm2, Gaa, Fndc5, and Irisin (Figures 3C and 3D). Together, these *in vitro* overexpression experiments identify principal mediators through which miR-27a-3p and miR-142-3p might exert their differential control of fuel consumption in muscle cells.

miR-27a-3p and miR-142-3p Control Fuel Availability *In Vivo*

To test whether these two miRNAs can also induce glycogen or lipid accumulation *in vivo*, we transfected hindlimb mouse muscles with miRNA mimics, obtaining an overexpression of at least



(legend on next page)

1.5 times (Figure 4A). qRT-PCR experiments on transfected muscles confirmed the reduced expression of the miRNA targets identified by *in vitro* experiments (Pgm2, Gaa, and Fndc5) (Figure 4B). Furthermore, other master genes involved in FA metabolism, such as *Cpt2*, *Plin2*, and *Lipe*, were downregulated in muscles following miR-142-3p transfection.

In muscle overexpressing miR-27a-3p, periodic acid-Schiff (PAS) staining confirmed glycogen accumulation (Figures 4D and 4E). Electron microscopy confirmed the presence of abundant glycogen granules and showed that mitochondria were impaired but generally maintained regular cristae structure (Figure 4F).

The expression of miR-142-3p *in vivo* recapitulated the results obtained in C2C12 myoblasts, with stronger BODIPY staining when muscles were transfected with the miRNA mimic (Figures 4G and 4H) and evident lipid droplets in electron microscopy images (Figure 4F). Because the impairment of nutrient availability causes mitochondrial alterations paralleled by variation in the expression of genes involved in mitochondrial fusion-fission (Galloway and Yoon, 2012; Liesa and Shirihai, 2013), we analyzed the expression of specific genes involved in the regulation of mitochondrial networks. We found that *Mfn2* was slightly downregulated after the overexpression of miR-27a-3p (Figure 4C), even though this family of genes did not appear as a target of both miRNAs in our network analysis. *Mfn2* is involved in mitochondrial fusion, and miR-27a-3p overexpression in C2C12 cells induced mitochondrial fragmentation (Figure 2C). When miR-142-3p was upregulated, overexpression of *Fis1*,

involved in mitochondrial fission, was associated with the overexpression of *Mfn1* and *Opa1*, both of which are involved in mitochondrial fusion (Figure 4C).

Interestingly, upon miR-27a-3p overexpression, succinate dehydrogenase staining indicated an increase in oxidative myofibers and a reduction in glycolytic myofibers, in agreement with the overexpression of mRNAs for oxidative enzymes in tl myofibers. No such variations were observed in muscles transfected with miR-142-3p (Figures 4I and 4J). We analyzed the expression of *Myh2* gene, coding for MyHC protein that is specifically expressed in the most oxidative type 2A myofibers, following the overexpression of miR-27a-3p and miR-142-3p. We noted an upregulation of *Myh2* only after the overexpression of the miR-27a-3p (Figure 4K). To confirm that overexpression of miR-27a-3p increases the number of type 2A myofibers, we stained transfected muscles for MyHC-2A (Figure 4L). Fiber counting confirmed an increased number of type 2A myofibers following overexpression of the miR-27a-3p. In contrast, overexpression of miR-142-3p did not affect the number of type 2A myofibers (Figure 4M), consistent with its neutral effect on the number of SDH-positive myofibers (Figure 4I).

Because HFD can induce obesity and metabolic disorders in mice associated with lipid accumulation in muscles, we tested if the expression of miR-27a-3p and miR-142-3p were altered in the muscles of HFD mice. The expression of miR-27a-3p increased in all tested muscles derived from HFD mice, while miR-142-3p decreased in all muscles tested except EDL (Figure 5A). The opposite expression patterns of miR-27a-3p and

Figure 4. Alterations of Fuel Availability Induced by miR-27a-3p and miR-142-3p: *In Vivo* Studies

(A) Relative quantification (RQ) by qRT-PCR of miR-27a-3p and miR-142-3p transcripts after muscle transfection. Results are represented as the average between gastrocnemius and tibialis anterior (TA) of three mice. p values from t tests are indicated as follows: *p < 0.05.

(B) RQ by qRT-PCR of specific transcripts, coding for relevant metabolic enzymes, in mouse EDL muscles transfected with miR-27a-3p or miR-142-3p mimics. These *in vivo* experiments confirm that (1) miR-27a-3p upregulation affects the expression of *Pgm2* and *Gaa* genes, and (2) miR-142-3p upregulation diminishes the expression of *Fndc5* and *Cpt2*. Moreover, when miR-142-3p is upregulated in muscles, *Plin2*, a marker of lipid droplets, is overexpressed, and the lipase hormone sensitive (*Lipe*) is under-expressed. Each experiment was performed in three muscles of different mice in three technical replicates. Error bars are SEM. p values from t tests are indicated as follows: *p < 0.05 and ***p < 0.001.

(C) RQ of transcripts coding for proteins involved in the regulation of mitochondrial dynamics after miR-27a-3p and miR-142-3p overexpression in three different tibialis anterior muscles. *Fis1* participates in mitochondrial fission, whereas *Mfn1*, *Mfn2*, and *Opa1* participate in mitochondrial fusion. p values from t tests are indicated as follows: *p < 0.05 and ***p < 0.001.

(D) Representative cross sections of mouse tibialis anterior stained with PAS to detect glycogen after 1 week of transfection with a scramble sequence as control (Scr), with miR-27a-3p or with miR-142-3p. Scale bar is 200 μ m.

(E) The intensities of PAS color pixel were graphed in Tukey boxplots. PAS intensity color increased in cross section of muscles transfected with miR-27a-3p. p value from t test is indicated as follows: ***p < 0.001.

(F) Electron microscopy of longitudinal (LONG.) and transverse (TRANSV.; inset) sections of transfected gastrocnemius muscles. Arrows indicate glycogen granules in muscles overexpressing miR-27a-3p or lipid droplets in muscles overexpressing miR-142-3p. Scale bar is 500 nm.

(G) Representative cross sections of mouse TA stained for lipids with BODIPY after 1 week of transfection with a scramble sequence as control, with miR-27a-3p or with miR-142-3p. Scale bar is 50 μ m.

(H) BODIPY fluorescence pixel intensities were graphed in Tukey boxplots. Number of independent experiments (n) per condition = 3. p value from t test is indicated as follows: ***p < 0.001.

(I) Representative cross section of mouse muscle gastrocnemius after 1 week of transfection. Oxidative myofibers are positive to succinate dehydrogenase (SDH) staining (blue). Scale bar is 100 μ m.

(J) Quantification of SDH-positive fibers. At least 2,500 fibers were analyzed for each transfection. Error bars are SEM. Adjusted p values from ANOVA (in comparison with control) are indicated as follows: *p < 0.05.

(K) Relative expression of *Myh2* (coding for MyHC-2A, the marker of type 2A myofibers) in three TA muscles after transfection with miR-27a-3p and miR-142-3p. p value from t test is indicated as follows: ***p < 0.001.

(L) Cross-sectional area of TA mouse muscle stained for MyHC-2A (green) and dystrophin (red) after transfection of miR-27a-3p or miR-142-3p. Scale bars are 200 μ m.

(M) Frequency of type 2A myofibers in TA mouse muscles after transfection of miR-27a-3p or miR-142-3p. SEM is represented. p value from t test is indicated as follows: *p < 0.05.

Three independent transfections were performed in three mice.

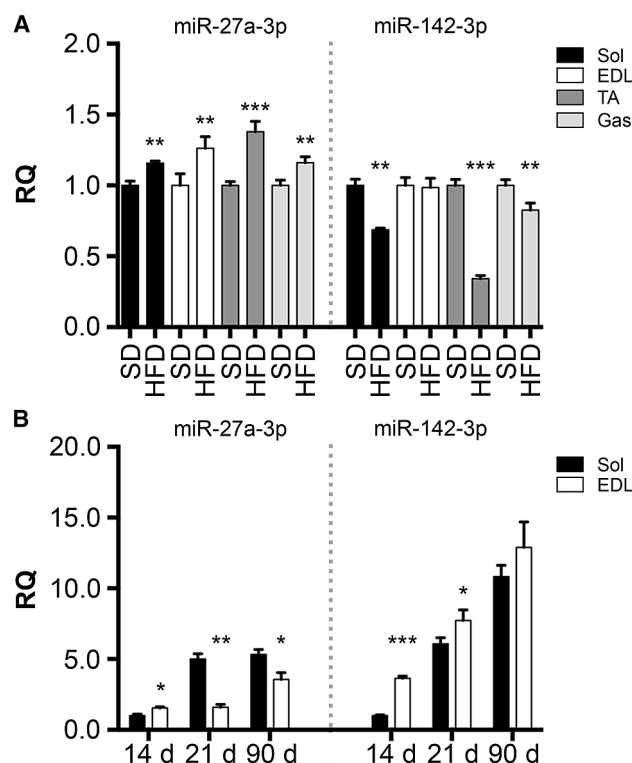


Figure 5. Expression of miR-27a-3p and miR-142-3p
(A) Relative quantification (RQ) by qRT-PCR of miR-27a-3p and miR-142-3p in soleus (Sol), EDL, TA, and gastrocnemius (Gas) of mice fed with a high-fat diet (HFD) in comparison with mice fed with a standard diet (SD).
(B) RQ by qRT-PCR of miR-27a-3p and miR-142-3p at different time points of skeletal muscle development: 14, 21, and 90 days (d) after birth. Results are represented as the average among three biological and technical replicates. Error bars are SEM. p values are indicated as follows: *p < 0.05, **p < 0.01, and ***p < 0.001.

miR-142-3p in muscles from HFD mice support their different functions in the maintenance of lipid content in muscle. We observed that after miR-27a-3p overexpression, lipid content decreased, while after miR-142-3p overexpression, lipid content increased (Figure 4H). This observation is consistent with the activation of miR-27a-3p and the inhibition of miR-142-3p noted in muscles with increased lipid content such as those from HFD mice to allow lipid consumption and avoid a surplus accumulation.

In summary, our collective *in vitro* and *in vivo* results were consistent in suggesting differential roles of miR-27a-3p and miR-142-3p in the regulation of fuel consumption in skeletal muscle.

Finally, we analyzed the expression of miR-27a-3p and miR-142-3p during postnatal muscle development. Interestingly, we observed that miR-27a-3p can alter the number of type 2A myofibers when overexpressed. In the mouse soleus, type 2A myofibers first appear 7 days after birth, reaching their peak after 21 days. In EDL, type 2A fibers are absent, with the exception of a small number of muscles of 21-day-old mice (Agbulut et al., 2003). We noted that the expression of miR-27a-3p increased faster in soleus than in EDL, and its high expression was maintained in adult mice (Fig-

ure 5B). This result may be related to the ability of miR-27a-3p to promote the formation of type 2A myofibers. On the contrary, miR-142-3p lost its differential expression among soleus and EDL during development (Figure 5B).

DISCUSSION

In this work, we describe how the metabolic plasticity of myofibers relies on dynamic transcriptional networks that govern their fuel preferences, and by generating and examining the compendium of mRNAs and miRNAs expressed in single isolated myofibers from mouse muscles, we identify two miRNAs that can modulate lipid use in myofibers.

Previous transcriptional catalogs obtained from whole-muscle samples (Campbell et al., 2001; Raz et al., 2018; Wu et al., 2003) represent an average transcriptome of the different muscle cell repertoires and lack the resolution power to identify the specific signatures of different myofiber types. Therefore, the evolution of single-cell approaches allows the identification of signatures that specify functional and metabolic behavior of individual myofiber types. Our analysis of transcriptional signatures shows that the preferential metabolism (oxidative or glycolytic) is a key component that describes the myofiber molecular phenotype. tS and tI myofibers display high expression levels of genes encoding for enzymes of oxidative phosphorylation and FA oxidation, whereas tF myofibers preferentially express genes encoding enzymes for glycolytic metabolism. This picture is closer to the more traditional functional classification of muscle myofibers, which differentiates them as slow oxidative, fast oxidative, and fast glycolytic (Peter et al., 1972), than to the MyHC-based classification. In addition, although this work was performed using mouse muscles, the three transcriptional signatures in which mouse myofibers were divided clearly evoke the three types of human myofibers, in which the most fast-glycolytic MyHC is not expressed. Interestingly, we observed that tI myofibers are characterized by the highest level of expression of genes coding for mitochondrial enzymes. This observation agrees with a previous proteomic analysis of single myofibers (Murgia et al., 2015) that identified an enrichment of mitochondrial proteins involved in oxidative phosphorylation in type 2A fibers, in accordance with their largest content in mitochondria (Schiaffino et al., 1970).

To profile non-coding RNAs and to assign them a role in a specific myofiber subtype, miRNA and mRNA expression profiles must be integrated. With this approach we identified post-transcriptional circuits involved in the regulation of myofiber metabolism, in addition to those already established involving miR-208b-3p, miR-499-5p, and Sox6 (Gan et al., 2013; van Rooij et al., 2009). Our integrated approach highlights two previously unappreciated major circuits that connect metabolic transcripts with miR-27a-3p and miR-142-3p. The single-myofiber approach revealed their opposite expression in the tI myofibers, miR-27a-3p being highly and miR-142-3p lowly expressed. This set of findings suggests a complementary effect of these two miRNAs in regulating myofiber metabolism. Both *in vitro* and *in vivo* functional assays revealed that miR-27a-3p improves lipid use and reduces the breakdown of glycogen and consequently glycolysis (Figure 6A). These adaptations in the selection of a specific fuel source due to miR-27a-3p are consistent with the

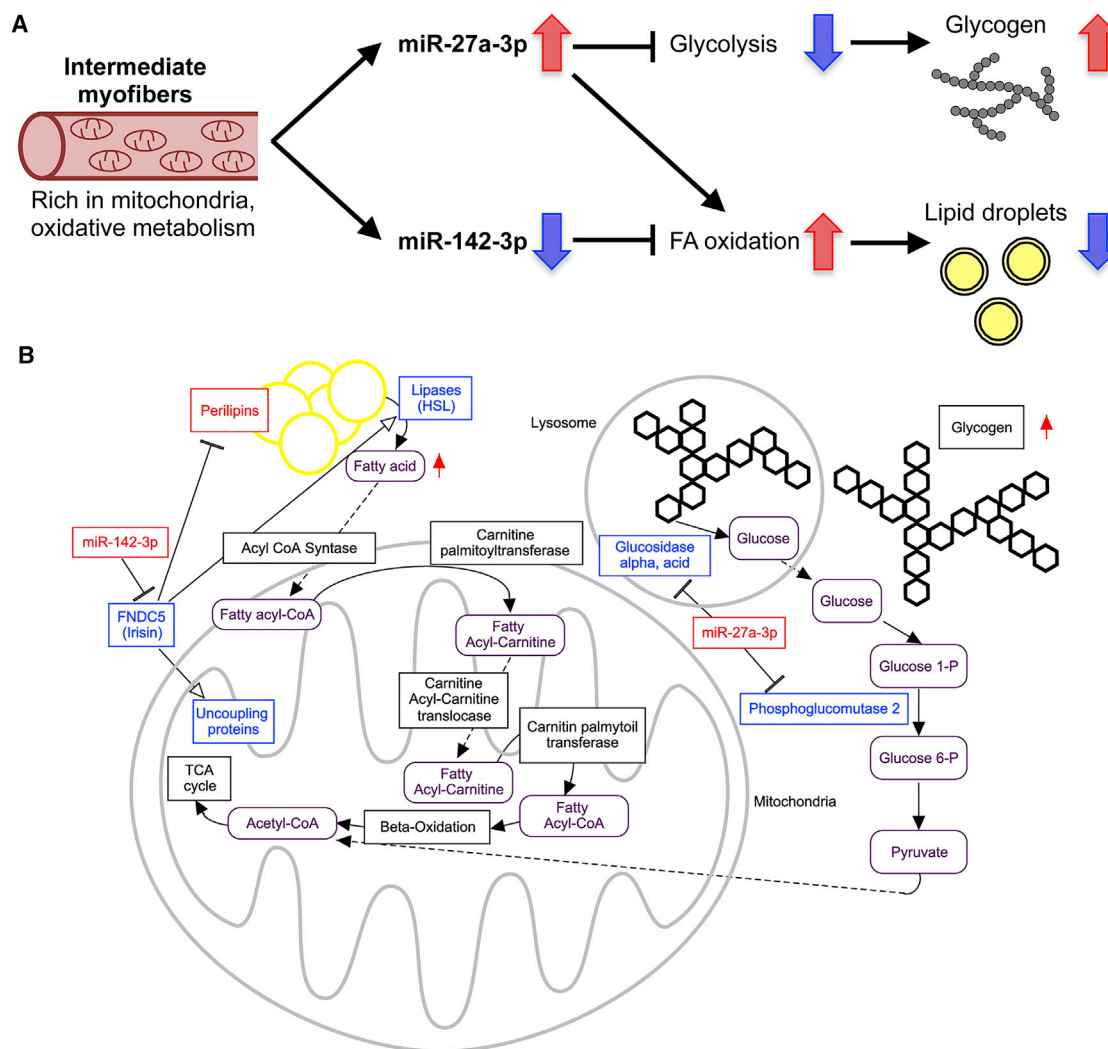


Figure 6. Role of miR-27a-3p and miR-142-3p in Myofiber Metabolism

(A) Model integrating the circuits by which miR-27a-3p and miR-142-3p orchestrate glycogen and FA metabolism in tl myofibers.

(B) A more detailed scheme representing miRNA modulation of myofiber metabolism. For all components of the scheme, blue indicates low levels and red high levels. Asterisks indicate the miRNAs of interest.

oxidative metabolism of tl myofibers and help explain the ability of the miRNA to change the myofiber phenotype from glycolytic to oxidative. In contrast, miR-142-3p inhibits lipid use in myofibers (Figure 6A). However, tS myofibers, which use lipids as fuel, also express miR-142-3p, suggesting that the different repertoire of miRNA expression in tS and tl fibers can differently influence genes involved in lipid catabolism.

Increased miRNAs dose leads to accumulation of unused nutrients (i.e., glycogen and lipids) and to mitochondrial fragmentation. Although changes in morphology appear ancillary, mitochondrial fuel use is conversely embedded in the program controlled by these metabolic signatures. Expression of miR-27a-3p results in reduced maximal mitochondrial respiration and in glycogen accumulation due to inhibition of cytosolic and lysosomal glycogen breakdown. Indeed, we found that miR-27a-3p expression represses Pgm2 (an enzyme involved in the

conversion of glucose 1 phosphate generated by the Pgm into glucose 6 phosphate) and Gaa (a lysosomal enzyme essential for the hydrolysis of glycogen to glucose) (Figure 6B). Concomitantly, miR-27a-3p improves lipid use, supporting its established role in adipocytes and hepatocytes (Ji et al., 2009; Shirasaki et al., 2013; Wang et al., 2011).

miR-142-3p impairs FA use, resulting in the accumulation of lipid droplets. Indeed, miR-142-3p expression is lowest in tl myofibers, characterized by the highest expression of mitochondrial genes. Conversely, miR-142-3p overexpression shuts down the FA mitochondrial transporter carnitine palmitoyltransferase and the uncoupling proteins Ucp2 and Ucp3. Ucp3 prevents triglyceride storage (Musa et al., 2012), and its expression increases in C2C12 myoblasts exposed to the myokine Irisin (Vaughan et al., 2014). Interestingly, the Irisin precursor Fndc5 is the most downregulated transcript among miR-142-3p targets (Figure 6B).

miR-142-3p therefore emerges as a crucial molecule controlling the Fndc5-Irisin pathway as it inhibits Irisin autocrine effects, thereby impairing FA use, leading to lipid droplet accumulation. Indeed, miR-142-3p downregulates HSL and upregulates perilipins, whereas Fndc5-Irisin promotes lipolysis by triggering the opposite effect on HSL and perilipins (Xiong et al., 2015).

The miRNAs and targets discovered in our work are likely participants in obesity and diabetes. Indeed, a rat model of type 2 diabetes and mature adipocytes from obese mice display deregulation of miR-27a-3p as well as of its target Gpd2 (Herrera et al., 2010; MacDonald et al., 1996). miR-142-3p was associated with alterations in lipid pathways and abnormal fat deposition in brain (Lau et al., 2013) and is a biomarker for morbidity of obesity and type 2 diabetes (Ortega et al., 2013, 2014). We can envision that muscular metabolic reprogramming by delivery of the miRNAs or antagomirs detailed in this work could be a promising route for the development of treatments counteracting the pathological side effects of diabetes and obesity. Importantly miR-27a-3p was upregulated in muscles from HFD mice, while miR-142-3p was downregulated, supporting a compensatory effect to avoid further lipid accumulation.

STAR★METHODS

Detailed methods are provided in the online version of this paper and include the following:

- KEY RESOURCES TABLE
- CONTACT FOR REAGENT AND RESOURCE SHARING
- EXPERIMENTAL MODEL AND SUBJECT DETAILS
 - Mice
 - Culture cells
- METHODS DETAILS
 - Mouse and Tissue Handling
 - Screening of soleus and EDL myofibers
 - RNA isolation
 - Microarray profiles
 - mRNA qRT-PCR
 - miRNA qRT-PCR
 - NGS of miRNAs purified from single myofibers
 - miRNA overexpression
 - Imaging
- QUANTIFICATION AND STATISTICAL ANALYSIS
 - Microarray data analysis
 - Sequencing data processing
 - Analysis of miRNA families
 - Construction of mRNA-miRNA network
 - Statistical analysis
 - qRT-PCR data analysis
 - Image analysis
 - Western blot analysis
 - Lipidomic analysis
- DATA AND SOFTWARE AVAILABILITY

SUPPLEMENTAL INFORMATION

Supplemental Information can be found with this article online at <https://doi.org/10.1016/j.celrep.2019.02.105>.

ACKNOWLEDGMENTS

We wish to thank Dr. Federico Caicci (Biolmaging Facility of the Department of Biology, University of Padova) for help with electron microscopy analyses; Dr. Caterina Millino and Dr. Beniamina Pacchioni (Microarray Service Micro-Cribi, CRIBI Biotechnology Centre, University of Padova) for the help with microarray analyses; Anna Stocco for her commitment in performing preliminary experiments; Professor Fabio Di Lisa and Dr. Valeria Petronilli for useful discussions; and Dr. Kelly Carroll and Dr. Catherine Makarewicz for critical reading of the manuscript. This work was supported by grants from the CARIPARO Foundation (FIBRE-GEXP) and the University of Padova (CPDA139317) to S.C. and G.L.; the Cariplo Foundation (2016-1006) to S.C. and G.L.; the Italian Ministry of Health (GR-2011-02346845) to S.C.; the AIRC Foundation (Italy project IG2015-ID17773) to G.L.; an FP7 CIG (PCIG13-GA-2013-618697); the Italian Ministry of Research (FIRB RBAP1123YA_005); and a grant from the EFSD/Novo Nordisk Programme for Diabetes Research in Europe to L.S. F.G. and E.H.-C. were supported by a DTI-IMPORT FP7 fellowship.

AUTHOR CONTRIBUTIONS

G.L., C. Reggiani, L.S., and S.C. conceived the project. F.C., F.G., A.Z., P.C., E.H.-C., P.M., C.B., E.A., L.B., A.A., and R.F. performed experiments. F.C., P.L., G.G., C. Romualdi, P.B., M.S., L.S., S.C., and G.L. analyzed results. F.C., S.C., L.S., P.B., and G.L. wrote the manuscript, which all authors reviewed.

DECLARATION OF INTERESTS

The authors declare no competing interests.

Received: March 5, 2018

Revised: June 29, 2018

Accepted: February 26, 2019

Published: March 26, 2019

REFERENCES

- Agbulut, O., Noirez, P., Beaumont, F., and Butler-Browne, G. (2003). Myosin heavy chain isoforms in postnatal muscle development of mice. *Biol. Cell* 95, 399–406.
- Bean, C., Facchinello, N., Faulkner, G., and Lanfranchi, G. (2008). The effects of Ankrd2 alteration indicate its involvement in cell cycle regulation during muscle differentiation. *Biochim. Biophys. Acta* 1783, 1023–1035.
- Betel, D., Koppal, A., Agius, P., Sander, C., and Leslie, C. (2010). Comprehensive modeling of microRNA targets predicts functional non-conserved and non-canonical sites. *Genome Biol.* 11, R90.
- Biscontin, A., Casara, S., Cagnin, S., Tombolan, L., Rosolen, A., Lanfranchi, G., and De Pittà, C. (2010). New miRNA labeling method for bead-based quantification. *BMC Mol. Biol.* 11, 44.
- Blanco, C.E., Sieck, G.C., and Edgerton, V.R. (1988). Quantitative histochemical determination of succinic dehydrogenase activity in skeletal muscle fibres. *Histochem. J.* 20, 230–243.
- Boettger, T., Wüst, S., Nolte, H., and Braun, T. (2014). The miR-206/133b cluster is dispensable for development, survival and regeneration of skeletal muscle. *Skelet. Muscle* 4, 23.
- Boström, P., Wu, J., Jedrychowski, M.P., Korde, A., Ye, L., Lo, J.C., Rasbach, K.A., Boström, E.A., Choi, J.H., Long, J.Z., et al. (2012). A PGC1- α -dependent myokine that drives brown-fat-like development of white fat and thermogenesis. *Nature* 481, 463–468.
- Campbell, W.G., Gordon, S.E., Carlson, C.J., Pattison, J.S., Hamilton, M.T., and Booth, F.W. (2001). Differential global gene expression in red and white skeletal muscle. *Am. J. Physiol. Cell Physiol.* 280, C763–C768.
- Carrasco, M.A., and Hidalgo, C. (2006). Calcium microdomains and gene expression in neurons and skeletal muscle cells. *Cell Calcium* 40, 575–583.

- Carrer, M., Liu, N., Grueter, C.E., Williams, A.H., Frisard, M.I., Hulver, M.W., Bassel-Duby, R., and Olson, E.N. (2012). Control of mitochondrial metabolism and systemic energy homeostasis by microRNAs 378 and 378*. *Proc. Natl. Acad. Sci. U S A* 109, 15330–15335.
- Chemello, F., Bean, C., Cancellara, P., Laveder, P., Reggiani, C., and Lanfranchi, G. (2011). Microgenomic analysis in skeletal muscle: expression signatures of individual fast and slow myofibers. *PLoS ONE* 6, e16807.
- Chemello, F., Mammucari, C., Gherardi, G., Rizzuto, R., Lanfranchi, G., and Cagnin, S. (2015). Gene expression changes of single skeletal muscle fibers in response to modulation of the mitochondrial calcium uniporter (MCU). *Genom. Data* 5, 64–67.
- de Lange, P., Moreno, M., Silvestri, E., Lombardi, A., Goglia, F., and Lanni, A. (2007). Fuel economy in food-deprived skeletal muscle: signaling pathways and regulatory mechanisms. *FASEB J.* 21, 3431–3441.
- Dumortier, O., Hinault, C., and Van Obberghen, E. (2013). MicroRNAs and metabolism crosstalk in energy homeostasis. *Cell Metab.* 18, 312–324.
- Egan, B., and Zierath, J.R. (2013). Exercise metabolism and the molecular regulation of skeletal muscle adaptation. *Cell Metab.* 17, 162–184.
- Fan, W., and Evans, R. (2015). PPARs and ERRs: molecular mediators of mitochondrial metabolism. *Curr. Opin. Cell Biol.* 33, 49–54.
- Friedländer, M.R., Chen, W., Adamidi, C., Maaskola, J., Einspanier, R., Knespel, S., and Rajewsky, N. (2008). Discovering microRNAs from deep sequencing data using miRDeep. *Nat. Biotechnol.* 26, 407–415.
- Friedman, R.C., Farh, K.K., Burge, C.B., and Bartel, D.P. (2009). Most mammalian mRNAs are conserved targets of microRNAs. *Genome Res.* 19, 92–105.
- Galloway, C.A., and Yoon, Y. (2012). Perspectives on: SGP symposium on mitochondrial physiology and medicine: what comes first, misshape or dysfunction? The view from metabolic excess. *J. Gen. Physiol.* 139, 455–463.
- Gan, Z., Rumsey, J., Hazen, B.C., Lai, L., Leone, T.C., Vega, R.B., Xie, H., Conley, K.E., Auwerx, J., Smith, S.R., et al. (2013). Nuclear receptor/microRNA circuitry links muscle fiber type to energy metabolism. *J. Clin. Invest.* 123, 2564–2575.
- Gilda, J.E., and Gomes, A.V. (2013). Stain-free total protein staining is a superior loading control to β -actin for western blots. *Anal. Biochem.* 440, 186–188.
- Griffiths-Jones, S. (2004). The microRNA Registry. *Nucleic Acids Res.* 32, D109–D111.
- Herrera, B.M., Lockstone, H.E., Taylor, J.M., Ria, M., Barrett, A., Collins, S., Kaisaki, P., Argoud, K., Fernandez, C., Travers, M.E., et al. (2010). Global microRNA expression profiles in insulin target tissues in a spontaneous rat model of type 2 diabetes. *Diabetologia* 53, 1099–1109.
- Hu, W., and Collier, J. (2012). What comes first: translational repression or mRNA degradation? The deepening mystery of microRNA function. *Cell Res.* 22, 1322–1324.
- Huang, W., Sherman, B.T., and Lempicki, R.A. (2009). Systematic and integrative analysis of large gene lists using DAVID bioinformatics resources. *Nat. Protoc.* 4, 44–57.
- Jensen, J., Rustad, P.I., Kolnes, A.J., and Lai, Y.C. (2011). The role of skeletal muscle glycogen breakdown for regulation of insulin sensitivity by exercise. *Front. Physiol.* 2, 112.
- Ji, J., Zhang, J., Huang, G., Qian, J., Wang, X., and Mei, S. (2009). Over-expressed microRNA-27a and 27b influence fat accumulation and cell proliferation during rat hepatic stellate cell activation. *FEBS Lett.* 583, 759–766.
- Jiang, J., Mo, H., Liu, C., Wu, B., Wu, Z., Li, X., Li, T., He, S., Li, S., You, Q., et al. (2018). Inhibition of miR-186-5p contributes to high glucose-induced injury in AC16 cardiomyocytes. *Exp. Ther. Med.* 15, 627–632.
- Lau, P., Bossers, K., Janky, R., Salta, E., Frigerio, C.S., Barbash, S., Rothman, R., Sierksma, A.S., Thathiah, A., Greenberg, D., et al. (2013). Alteration of the microRNA network during the progression of Alzheimer's disease. *EMBO Mol. Med.* 5, 1613–1634.
- Lee, E.K., Lee, M.J., Abdelmohsen, K., Kim, W., Kim, M.M., Srikantan, S., Martindale, J.L., Hutchison, E.R., Kim, H.H., Marasa, B.S., et al. (2011). miR-130 suppresses adipogenesis by inhibiting peroxisome proliferator-activated receptor gamma expression. *Mol. Cell. Biol.* 31, 626–638.
- Li, R., and Shen, Y. (2013). An old method facing a new challenge: re-visiting housekeeping proteins as internal reference control for neuroscience research. *Life Sci.* 92, 747–751.
- Li, L.O., Grevengoed, T.J., Paul, D.S., Ilkayeva, O., Koves, T.R., Pascual, F., Newgard, C.B., Muoio, D.M., and Coleman, R.A. (2015). Compartmentalized acyl-CoA metabolism in skeletal muscle regulates systemic glucose homeostasis. *Diabetes* 64, 23–35.
- Liesa, M., and Shrihai, O.S. (2013). Mitochondrial dynamics in the regulation of nutrient utilization and energy expenditure. *Cell Metab.* 17, 491–506.
- MacDonald, M.J., Tang, J., and Polonsky, K.S. (1996). Low mitochondrial glycerol phosphate dehydrogenase and pyruvate carboxylase in pancreatic islets of Zucker diabetic fatty rats. *Diabetes* 45, 1626–1630.
- Mammucari, C., Gherardi, G., Zamparo, I., Raffaello, A., Boncompagni, S., Chemello, F., Cagnin, S., Braga, A., Zanin, S., Pallafacchina, G., et al. (2015). The mitochondrial calcium uniporter controls skeletal muscle trophism in vivo. *Cell Rep.* 10, 1269–1279.
- Martini, P., Sales, G., Brugiolo, M., Gandaglia, A., Naso, F., De Pittà, C., Spina, M., Gerosa, G., Chemello, F., Romualdi, C., et al. (2014). Tissue-specific expression and regulatory networks of pig microRNAome. *PLoS ONE* 9, e89755.
- McCarthy, J.J. (2011). The MyomiR network in skeletal muscle plasticity. *Exerc. Sport Sci. Rev.* 39, 150–154.
- Mishra, P., Varuzhanyan, G., Pham, A.H., and Chan, D.C. (2015). Mitochondrial dynamics is a distinguishing feature of skeletal muscle fiber types and regulates organellar compartmentalization. *Cell Metab.* 22, 1033–1044.
- Moritz, C.P. (2017). Tubulin or not tubulin: heading toward total protein staining as loading control in western blots. *Proteomics* 17.
- Murgia, M., Nagaraj, N., Deshmukh, A.S., Zeiler, M., Cancellara, P., Moretti, I., Reggiani, C., Schiaffino, S., and Mann, M. (2015). Single muscle fiber proteomics reveals unexpected mitochondrial specialization. *EMBO Rep.* 16, 387–395.
- Musa, C.V., Mancini, A., Alfieri, A., Labruna, G., Valerio, G., Franzese, A., Pisanis, F., Licenziati, M.R., Sacchetti, L., and Buono, P. (2012). Four novel UCP3 gene variants associated with childhood obesity: effect on fatty acid oxidation and on prevention of triglyceride storage. *Int. J. Obes.* 36, 207–217.
- Ortega, F.J., Mercader, J.M., Catalán, V., Moreno-Navarrete, J.M., Pueyo, N., Sabater, M., Gómez-Ambrosi, J., Anglada, R., Fernández-Fernández, J.A., Ricart, W., et al. (2013). Targeting the circulating microRNA signature of obesity. *Clin. Chem.* 59, 781–792.
- Ortega, F.J., Mercader, J.M., Moreno-Navarrete, J.M., Rovira, O., Guerra, E., Esteve, E., Xifra, G., Martínez, C., Ricart, W., Rieusset, J., et al. (2014). Profiling of circulating microRNAs reveals common microRNAs linked to type 2 diabetes that change with insulin sensitization. *Diabetes Care* 37, 1375–1383.
- Pastore, N., Vainshtein, A., Klisch, T.J., Armani, A., Huynh, T., Herz, N.J., Polishchuk, E.V., Sandri, M., and Ballabio, A. (2017). TFE3 regulates whole-body energy metabolism in cooperation with TFEB. *EMBO Mol. Med.* 9, 605–621.
- Peter, J.B., Barnard, R.J., Edgerton, V.R., Gillespie, C.A., and Stempel, K.E. (1972). Metabolic profiles of three fiber types of skeletal muscle in guinea pigs and rabbits. *Biochemistry* 11, 2627–2633.
- Quiat, D., Voelker, K.A., Pei, J., Grishin, N.V., Grange, R.W., Bassel-Duby, R., and Olson, E.N. (2011). Concerted regulation of myofiber-specific gene expression and muscle performance by the transcriptional repressor Sox6. *Proc. Natl. Acad. Sci. U S A* 108, 10196–10201.
- Raz, V., Riaz, M., Tatum, Z., Kielbasa, S.M., and 't Hoen, P.A.C. (2018). The distinct transcriptomes of slow and fast adult muscles are delineated by non-coding RNAs. *FASEB J.* 32, 1579–1590.
- Rivero-Gutiérrez, B., Anzola, A., Martínez-Augustín, O., and de Medina, F.S. (2014). Stain-free detection as loading control alternative to Ponceau and housekeeping protein immunodetection in Western blotting. *Anal. Biochem.* 467, 1–3.

- Rottiers, V., and Nääär, A.M. (2012). MicroRNAs in metabolism and metabolic disorders. *Nat. Rev. Mol. Cell Biol.* **13**, 239–250.
- Saeed, A.I., Sharov, V., White, J., Li, J., Liang, W., Bhagabati, N., Braisted, J., Klapa, M., Currier, T., Thiagarajan, M., et al. (2003). TM4: a free, open-source system for microarray data management and analysis. *Biotechniques* **34**, 374–378.
- Schiaffino, S., and Reggiani, C. (2011). Fiber types in mammalian skeletal muscles. *Physiol. Rev.* **91**, 1447–1531.
- Schiaffino, S., Hanzlíková, V., and Pierobon, S. (1970). Relations between structure and function in rat skeletal muscle fibers. *J. Cell Biol.* **47**, 107–119.
- Schrepfer, E., and Scorrano, L. (2016). Mitofusins, from mitochondria to metabolism. *Mol. Cell* **61**, 683–694.
- Sears, B., and Perry, M. (2015). The role of fatty acids in insulin resistance. *Lipids Health Dis.* **14**, 121.
- Shannon, P., Markiel, A., Ozier, O., Baliga, N.S., Wang, J.T., Ramage, D., Amin, N., Schwikowski, B., and Ideker, T. (2003). Cytoscape: a software environment for integrated models of biomolecular interaction networks. *Genome Res.* **13**, 2498–2504.
- Sharan, R., Maron-Katz, A., and Shamir, R. (2003). CLICK and EXPANDER: a system for clustering and visualizing gene expression data. *Bioinformatics* **19**, 1787–1799.
- Shimoni, Y., Friedlander, G., Hetzroni, G., Niv, G., Altuvia, S., Biham, O., and Margalit, H. (2007). Regulation of gene expression by small non-coding RNAs: a quantitative view. *Mol. Syst. Biol.* **3**, 138.
- Shirasaki, T., Honda, M., Shimakami, T., Horii, R., Yamashita, T., Sakai, Y., Sakai, A., Okada, H., Watanabe, R., Murakami, S., et al. (2013). MicroRNA-27a regulates lipid metabolism and inhibits hepatitis C virus replication in human hepatoma cells. *J. Virol.* **87**, 5270–5286.
- Sun, P., Hu, J.W., Xiong, W.J., and Mi, J. (2014). miR-186 regulates glycolysis through Glut1 during the formation of cancer-associated fibroblasts. *Asian Pac. J. Cancer Prev.* **15**, 4245–4250.
- Tibshirani, R., Hastie, T., Narasimhan, B., and Chu, G. (2002). Diagnosis of multiple cancer types by shrunken centroids of gene expression. *Proc. Natl. Acad. Sci. U S A* **99**, 6567–6572.
- Tusher, V.G., Tibshirani, R., and Chu, G. (2001). Significance analysis of microarrays applied to the ionizing radiation response. *Proc. Natl. Acad. Sci. U S A* **98**, 5116–5121.
- Untergasser, A., Nijveen, H., Rao, X., Bisseling, T., Guerts, R., and Leunissen, J.A. (2007). Primer3Plus, an enhanced web interface to Primer3. *Nucleic Acids Res.* **35**, W71–W74.
- van Rooij, E., Quiat, D., Johnson, B.A., Sutherland, L.B., Qi, X., Richardson, J.A., Kelm, R.J., Jr., and Olson, E.N. (2009). A family of microRNAs encoded by myosin genes governs myosin expression and muscle performance. *Dev. Cell* **17**, 662–673.
- Vaughan, R.A., Gannon, N.P., Barberena, M.A., Garcia-Smith, R., Bisoffi, M., Mermier, C.M., Conn, C.A., and Trujillo, K.A. (2014). Characterization of the metabolic effects of irisin on skeletal muscle in vitro. *Diabetes Obes. Metab.* **16**, 711–718.
- Vowinckel, J., Hartl, J., Butler, R., and Ralser, M. (2015). MitoLoc: A method for the simultaneous quantification of mitochondrial network morphology and membrane potential in single cells. *Mitochondrion* **24**, 77–86.
- Wang, Q., Wang, Y., Minto, A.W., Wang, J., Shi, Q., Li, X., and Quigg, R.J. (2008). MicroRNA-377 is up-regulated and can lead to increased fibronectin production in diabetic nephropathy. *FASEB J.* **22**, 4126–4135.
- Wang, T., Li, M., Guan, J., Li, P., Wang, H., Guo, Y., Shuai, S., and Li, X. (2011). MicroRNAs miR-27a and miR-143 regulate porcine adipocyte lipid metabolism. *Int. J. Mol. Sci.* **12**, 7950–7959.
- Welinder, C., and Ekblad, L. (2011). Coomassie staining as loading control in Western blot analysis. *J. Proteome Res.* **10**, 1416–1419.
- Wu, H., Gallardo, T., Olson, E.N., Williams, R.S., and Shohet, R.V. (2003). Transcriptional analysis of mouse skeletal myofiber diversity and adaptation to endurance exercise. *J. Muscle Res. Cell Motil.* **24**, 587–592.
- Xiong, X.Q., Chen, D., Sun, H.J., Ding, L., Wang, J.J., Chen, Q., Li, Y.H., Zhou, Y.B., Han, Y., Zhang, F., et al. (2015). FNDC5 overexpression and irisin ameliorate glucose/lipid metabolic derangements and enhance lipolysis in obesity. *Biochim. Biophys. Acta* **1852**, 1867–1875.

STAR★METHODS

KEY RESOURCES TABLE

REAGENT or RESOURCE	SOURCE	IDENTIFIER
Antibodies		
Tom20 Antibody (FL-145)	Santa Cruz	sc-11415; RRID: AB_2207533
Goat anti-Rabbit IgG (H+L) Cross-Adsorbed Secondary Antibody, Alexa Fluor 568	Life Technologies	A-11011; RRID: AB_143157
Myosin Heavy Chain Type IIA Antibody	DSHB	SC-71; RRID: AB_2147165
Anti-Dystrophin antibody	Abcam	ab15277
Alexa Fluor® 488 AffiniPure Goat Anti-Mouse IgG, Fcγ subclass 1 specific	Jackson ImmunoResearch	115545205; RRID: AB_2338854
Alexa Fluor® 647 AffiniPure Goat Anti-Rabbit IgG (H+L)	Jackson ImmunoResearch	111605003; RRID: AB_2338072
Anti-GAA antibody produced in rabbit	Sigma-Aldrich	SAB2100872; RRID: AB_10604782
Anti-FNDC5 antibody [EPR12209]	Abcam	ab174833
Anti-FNDC5 antibody - C-terminal	Abcam	ab181884
Anti-PGM2 antibody [EPR10393(B)]	Abcam	ab151746
Rabbit IgG, HRP-linked whole Ab	Amersham	NA934; RRID: AB_772206
Bacterial and Virus Strains		
DH10b competent cells	ThermoFisher	18290015
Biological Samples		
<i>Soleus</i> Muscles	CD1 mice	N/A
EDL Muscles	CD1 mice	N/A
C2C12	ATCC	CRL-1772; RRID: CVCL_0188
Human primary myoblasts	ABM	T4068
Chemicals, Peptides, and Recombinant Proteins		
BODIPY 493/503	Life Technologies	D3922
Critical Commercial Assays		
Complete Whole Transcriptome Amplification Kit	Sigma-Aldrich	WTA2
SureTag DNA Labeling Kit	Agilent Technologies	5190-3400
Low Input Quick Amp Labeling Kit, one-color	Agilent Technologies	5190-2305
SurePrint G3 Mouse GE 8x60K Microarray Kit	Agilent Technologies	G4852A
Megaplex PreAmp Primers, Rodent Pool Set v3.0	Thermo Fischer Scientific	4444747
Megaplex RT Primers, Rodent Pool Set v3.0	Thermo Fischer Scientific	4444746
Seahorse XF Palmitate-BSA FAO Substrate	Seahorse Bioscience	102720-100
Deposited Data		
Agilent SurePrint G3 Mouse GE 8x60K Microarray Platform dataset	Agilent Technologies	https://www.ncbi.nlm.nih.gov/geo/query/acc.cgi?acc=GPL10787
miRBase, V.19	Griffiths-Jones, 2004	http://www.mirbase.org/
TargetScan, V.6.2	Friedman et al., 2009	www.targetscan.org/
mirSVR, August 2010 release	Betel et al., 2010	http://www.microrna.org/microrna/home.do
Raw microarray data	This paper	GEO: GSE98328
Raw miRNA-Seq fast myofibers	This paper	SRA: SRX2768351
Raw miRNA-Seq intermediate myofibers	This paper	SRA: SRX2768352
Raw miRNA-Seq slow myofibers	This paper	SRA: SRX2768353
Experimental Models: Cell Lines		
Mouse: C2C12	ATCC	CRL-1772; RRID: CVCL_0188
Human: Primary Skeletal Muscle Myoblasts	abm	T4068

(Continued on next page)

Continued

REAGENT or RESOURCE	SOURCE	IDENTIFIER
Experimental Models: Organisms/Strains		
Mouse: CD1	Charles River	CD-1 IGS Mouse
Mouse: C57BL/6J	The Jackson Laboratory	JAX: 000664
Oligonucleotides		
Primers for qRT-PCR: see Table S4	This paper	N/A
oligo-dT-Ion P1 Adaptor primer: CCTCTCTATGGGCAGTCGGTGATCCTCAGC[dT]20VN	This paper	N/A
SMART primer: CACACACAATTAACCCTCACTAAAggg	This paper	N/A
A Adaptor primer: CCATCTCATCCCTGCGTGTCTCCGACTCAG	This paper	N/A
Primers luciferase assay: see Table S4	This paper	N/A
Recombinant DNA		
PCMVIR MicroRNA Expression Vector	Origene	PCMVIR
PCMVIR-27a	Origene	SC400942
PCMVIR-142	Origene	SC400778
Mito-RFP	Evrogen	FP147
pmirGLO Dual-Luciferase miRNA Target Expression Vector	Promega	E1330
Software and Algorithms		
Primer3Plus	Untergasser et al., 2007	http://www.bioinformatics.nl/cgi-bin/primer3plus/primer3plus.cgi
Feature Extraction Software v. 10.7.3.1	Agilent Technologies	G4463AA
Expander	Sharan et al., 2003	http://acgt.cs.tau.ac.il/expander/
Multiple Experiment Viewer	Saeed et al., 2003	https://sourceforge.net/projects/mev-tm4/
SAM: Significance Analysis of Microarrays	Tusher et al., 2001	http://statweb.stanford.edu/~tibs/SAM/
DAVID Bioinformatics Resources	Huang et al., 2009	https://david.ncifcrf.gov/
PAM: Prediction Analysis for Microarrays	Tibshirani et al., 2002	http://statweb.stanford.edu/~tibs/PAM/
miRDeep	Friedländer et al., 2008	https://sourceforge.net/projects/mirdeepstar/
Cytoscape	Shannon et al., 2003	https://cytoscape.org/
Prism	Graphpad	https://www.graphpad.com/scientific-software/prism/
ExpressionSuite Software	Thermo Fischer Scientific	https://www.thermofisher.com/us/en/home/technical-resources/software-downloads/expressionsuite-software.html
ImageJ	NIH	https://imagej.nih.gov/ij/
MitoLoc	Vowinckel et al., 2015	https://www.gurdon.cam.ac.uk/institute-life/downloadspublic/imaging-plugins
Other		
Rodent Diet With 60 kcal% Fat	Research Diets	D12492

CONTACT FOR REAGENT AND RESOURCE SHARING

Further information and requests for reagents may be directed to and will be fulfilled by the Lead Contact, Gerolamo Lanfranchi (gerolamo.lanfranchi@unipd.it).

EXPERIMENTAL MODEL AND SUBJECT DETAILS

Mice

Mice were wild-type CD1 3 months age male mice (Charles River, weight: 33 – 35 g), housed in a normal environment, provided with food and water and killed by rapid cervical dislocation to minimize suffering. For HFD experiments, C57BL/6J mice were fed with a high fat diet (60% kJ from fat; Research Diets) for 14 weeks beginning at 12 weeks of age. Body weight was recorded weekly. As controls were used mice fed with a standard diet. All aspects of animal care and experimentation were performed in accordance

with the Guide for the Care and Use of Laboratory Animals published by the National Institutes of Health (NIH Publication No. 85-23, Revised 1996) and the Italian regulations (DL 116/92) concerning the maintenance and use of laboratory animals. Experimental procedures were approved by the Ethical Committee of the University of Padova. All efforts were made to minimize animal suffering.

Culture cells

C2C12 myoblasts were cultured in Dulbecco's Modified Eagle Medium with high glucose (Life Technologies) + 10% Fetal Bovine Serum (Life Technologies) in 10 cm dishes and split every 2 or 3 days before they reached 70% of confluence. Human primary myoblasts were purchased from Applied Biological Materials (ABM) and cultured in the PriCoat T25 flasks using the Prigrow medium at 37°C and 5% of CO₂. Cells were split before they reached 80% of confluence.

METHODS DETAILS

Mouse and Tissue Handling

Muscles were collected from both hindlimbs following standard surgical procedures.

Screening of soleus and EDL myofibers

Enzymatic dissociation and classification of myofibers from *soleus* and EDL mouse muscles were fully described in our previous work (Chemello et al., 2011). Briefly, after collagenase treatment, each single isolated myofiber was cut and about one-third was used for MyHC protein isoform classification by SDS-PAGE whereas the remaining part was immediately immersed in TRIzol Reagent (Thermo Fisher Scientific) for RNA purification. All myofibers were collected within 45 min. from muscle disaggregation. Myofibers used for microarray analysis were purified from 13 different *soleus* muscles derived from 13 mice and 10 different EDL muscles derived from 10 mice; for sequencing analysis from 3 different *soleus* and 3 EDL muscles derived from 3 mice.

RNA isolation

Single isolated myofibers were separately lysed in 250 µl of TRIzol Reagent (Thermo Fisher Scientific) and RNA was extracted in the aqueous phase following the manufacturer's instructions. 70% ethanol was added before column purification. For microarray experiments, total RNA was purified using the RNeasy Micro Kit (QIAGEN), whereas, for miRNA analyses, separation of small and large RNAs was performed combining it with the miRNeasy Mini Kit (QIAGEN) as suggested by manufacturer's protocol. RNAs from whole muscles or cells were isolated using the standard phenol-chloroform extraction with TRIzol Reagent (Thermo Fisher Scientific) followed by isopropanol precipitation.

Microarray profiles

Amplification and labeling of RNA from single fibers

RNA purified from a single myofiber was exponentially amplified using the TransPlex Whole Transcriptome Amplification 2 Kit (Sigma-Aldrich) in accordance with the manufacturer's instructions. RNA was reverse-transcribed in a cDNA library, and the library was amplified for 18 cycles, below the amplification "plateau" observed in a PCR test reaction. To remove the residual primers and nucleotides, amplification product was purified with the GenElute PCR Clean-up columns (Sigma-Aldrich). Resulting cDNA was quantified with Nanodrop ND-1000 spectrophotometer (Thermo Fisher Scientific). 2 µg of amplified-purified cDNA were directly labeled using the Genomic DNA Enzymatic Labeling Kit (Agilent Technologies) as described by the proprietary protocol. The kit uses random primers and the exo-Klenow fragment to directly label cDNA samples with Cy3-dUTP nucleotides. Labeled cDNA was purified using the Amicon 30kDa filters (Millipore) and quantified using NanoDrop ND-1000 spectrophotometer (Thermo Fisher Scientific). On average, cDNA yield was about 4 µg and the specific activity was of 30 pmol Cy3 per µg cDNA.

Amplification and labeling of RNA from cells

RNAs obtained from cells were amplified and labeled starting from 150 ng and using the Low Input Quick Amp Labeling Kit, one-color (Agilent Technologies) as described by the proprietary protocol. Labeled cRNA was purified with miRNeasy Mini Kit (QIAGEN) and quantified using NanoDrop ND-1000 spectrophotometer (Thermo Fisher Scientific). On average, cRNA yield was about 10 µg and the specific activity was of 35 pmol Cy3 per µg cRNA.

Hybridization

Microarray experiments were performed with SurePrint G3 Mouse Gene Expression 8x60K microarray platforms (Agilent Technologies) containing 8 arrays per slide and consisting of 39,430 60-mer oligonucleotide probes for Entrez Gene RNAs (GPL10787). 800 ng of labeled sample targets were mixed with 5 µl of 10X Blocking Agent (Agilent Technologies) and water to a final volume of 25 µl. Samples were denatured at 95°C for 2 min. and added to 25 µl of 2X GEx Hybridization Buffer HI-RPM (Agilent Technologies). 40 µl mix was dispensed onto the array. Slides were loaded into the Agilent SureHyb chambers and hybridization was performed in a hybridization oven at 65°C for 17 hours with 10 rpm rotation. Finally, slides were washed using Wash Buffer Kit (Agilent Technologies) and dried at room temperature. Microarray slides were scanned using G2505C scanner (Agilent Technologies) at 3 µm resolution.

mRNA qRT-PCR

Primer design

qRT-PCR primers (Table S4) were designed by the primer design program Primer3Plus. All primer pairs span intron-exon boundaries. The specificity of each amplicon was assessed by dissociation curve analysis.

Reverse transcription

First-strand cDNA was synthesized following SuperScript III (Thermo Fisher Scientific) protocol in a total volume of 30 μ l. Oligo-dT was used for reverse transcription for all samples.

qRT-PCR reaction

SYBR Green technology was applied for all the assays with ABI 7500 Standard qRT-PCR System (Thermo Fisher Scientific). The total reaction volume was 10 μ l, including 5 μ l 2X GoTaq qPCR Master Mix (Promega), 0.6 μ l of 10 μ M left primer, 0.6 μ l of 10 μ M right primer, 1 μ l cDNA template, and 2.8 μ l of water. Each assay was performed in triplicate. Negative controls without template were added each time. The PCR program started with 2 min. at 95°C, followed by 40 cycles of two temperature steps (95°C, 15 s.; 60°C, 1 min.) and ended with 15 s. at 95°C, 1 min. at 60°C, 15 s. at 95°C and, 15 s. at 60°C. The last steps of PCR are performed to acquire the dissociation curve, validating the specificity of the PCR products.

miRNA qRT-PCR

Reverse transcription

The volume of miRNA population purified from a single myofiber was reduced by speed vacuum concentrator to 6 μ l and split in two portions. First-strand cDNA was synthesized using the Megaplex RT Primers Rodents Pools A and B (Thermo Fisher Scientific) and the TaqMan MicroRNA Reverse Transcription Kit (Thermo Fisher Scientific) following the corresponding protocol. To analyze miRNA expression in whole muscles 10 ng of total RNA were retrotranscribed using the TaqMan MicroRNA Reverse Transcription Kit (Thermo Fisher Scientific) as specified by the manufacturer.

Preamplification reaction

As miRNA amount purified from a single myofiber is very low, specific cDNA targets were amplified to increase the quantity of desired cDNA for expression analysis. This preamplification step was not performed in the case of whole muscles analyses. Preamplification was performed using TaqMan PreAmp Master Mix Kit (Thermo Fisher Scientific) and Megaplex PreAmp Primers Rodents Pools A and B (Thermo Fisher Scientific) in accordance with the manufacturer's instructions. For each transcriptional signature, pools of three cDNAs from isolated myofibers were prepared for qRT-PCR experiments.

qRT-PCR

qRT-PCR reactions were performed using TaqMan Universal Master Mix II, no UNG (Thermo Fisher Scientific) and a different TaqMan Small RNA Assay (Thermo Fisher Scientific) for each miRNA analyzed. Three replicates were performed for each reaction. Small nuclear RNA U6 was used as endogenous control, and negative controls without template were added in each plate. Reactions were run in ABI 7500 Standard qRT-PCR System (Thermo Fisher Scientific) with the following program: 95°C, 10 min; 35 cycles of 95°C 15 s. and 60°C 1 min.

NGS of miRNAs purified from single myofibers

Preparation of libraries

miRNAs libraries preparation partially follows previously set up method for miRNA labeling (Biscontin et al., 2010). Volume of miRNA population purified from a single myofibers was reduced by speed vacuum concentrator to 6.5 μ l. miRNAs were polyadenylated at 3' end using the Poly(A) Tailing Kit (Thermo Fisher Scientific), scaling the volumes of reagents in order to perform the reaction in 10 μ l. Polyadenylated miRNA molecules were precipitated with NaOAc 3 M pH 5.5 (1/10 volume) and absolute ethanol (4 volumes) overnight at -20°C and resuspended in 3.2 μ l of water. First-strand cDNA was synthesized using SuperScript II (Thermo Fisher Scientific) in a final volume of 10 μ l, including 10 pmol of oligo-dT-Ion P1 Adaptor primer (5'-CCTCTCTATGGGCAGTCGGTGATCCT CAGC[dT]20VN-3') and 50 pmol of SMART primer (5'-CACACACAATTAACCCTCACTAAAggg-3'). ssDNAs having a SMART anchor sequence at the 5' end was exponentially amplified by 10 PCR cycles performed with Platinum Taq DNA Polymerase High Fidelity (Thermo Fisher Scientific) using as right primer P1 and left primer an A Adaptor primer (5'-CCATCTCATCCCTGCGTGTCTCCGACT CAG-3') plus a barcode sequence specific for each myofiber type (tS: AAGAG; tI: TACCA; tF: CAGAA) plus SMART primer. A second step of PCR amplification was performed for 10 cycles using as primers A and P1. After each PCR reaction, products were purified twice through GenElute PCR Clean-up columns (Sigma-Aldrich) to eliminate primer-dimers. Library size selection was performed using E-Gel SizeSelect Gels (Thermo Fisher Scientific), according to manufacturer protocol, and recovering dsDNA longer than 120 nucleotides and shorter than 160.

Sequencing

Different tagged libraries were pooled together and used for emulsion PCR. Samples were loaded on the Ion OneTouch System (Thermo Fisher Scientific) according to manufacturer specifications and template-positive beads were purified through the Ion OneTouch ES (Thermo Fisher Scientific). Enriched beads were used to load 3 Ion PGM Chips (Thermo Fisher Scientific) and sequencing runs were performed using Ion PGM Sequencer (Thermo Fisher Scientific) according to manufacturer's protocol.

miRNA overexpression

Both C2C12 and human myoblasts were transfected using Lipofectamine 2000 (Life Technologies) following the manufacturer's instructions with 150 nM of mirVana miRNA mimics or scrambled sequence, purchased from Life Technologies. Transfection efficiency was evaluated with Ambion Silencer FAM-Labeled Negative Control (Life Technologies) and estimated of about 60% by fluorescence microscopy and flow cytometry. Each transfection experiment was independently repeated at least in triplicate. To obtain myotubes overexpressing miR-27a-3p and -142-3p, C2C12 myoblasts stably expressing both miRNAs using pCMV-MIR vectors (Origene) were purchased. 60,000 cells seeded in a well of 24 well plate were transfected with 1 μ g of plasmid using as transfecting agent the TransIT-X2 (Mirus) following the manufacturer protocol. 24 hours post-transfection, cells were put under selection with G418 antibiotic [0.5 mg/ml]. When cells were confluent, they were passed in wider plates (12 and 6 wells plates) in order to expand the cell lines. After one week of selection, antibiotic concentration was reduced to 0.3 mg/ml in order to maintain the selection pressure and reduce cell toxicity. After 2–3 weeks of selection, G418 was removed and cells were grown in proliferative medium. Differentiation was induced by switching from proliferation medium to differentiation medium (DMEM, 2% horse serum, 1 unit/ml Penicillin, 100 μ g/ml Streptomycin) upon reaching confluence and protracted until 7 days. Hindlimb mouse muscles were transfected using InvivoFectamine 2.0 (Life Technologies). Briefly, miRNA mimics were diluted to 0.5 mg/ml using complexation buffer, mixed to an equal volume of InvivoFectamine, and incubated at 50°C for 30 min. Immediately 80 μ l were injected in hindlimb muscles. Injection was repeated after 3 days and muscles were collected for analyses after one week from the first injection. Each transfection experiment was independently repeated at least in triplicate. For myosin staining after miRNAs overexpression, *in vivo* electroporation with pCMV-MIR recombinant vectors (Origene) was performed on TA muscles of three different mice. The muscle was isolated through a small hind limb incision, and 25 μ g of the same plasmids used to produce C2C12 stably expressing miRNAs were injected along the muscle length. Electric pulse was then applied by two stainless steel spatula electrodes placed on each side of the isolated muscle belly (50 V/cm, 5 pulses, 20 ms length, 200 ms intervals). Muscles were analyzed 21 days later in order to avoid evidences for inflammation or regeneration. After dissection, muscles were collected, immediately snap frozen in liquid nitrogen and conserved at –80°C as reported in (Pastore et al., 2017).

Imaging

Immunostaining

1x10⁴ C2C12 myoblasts were grown on 13 mm round coverslip in 25 mM glucose DMEM or FA oxidation medium (for the complete description see Seahorse analyses) and transfected as indicated. Following 72 hours of incubation, cells were fixed for 15 min. at room temperature with 4% ice-cold formaldehyde. Mitochondria of cells were stained with previously co-transfection with mito-RFP or with anti-TOM20. For anti-TOM20 staining, cells were permeabilized for 10 min. with 0.5% Triton X-100, blocked for 1 hour with 3% BSA in PBS, and then stained overnight at 4°C with a rabbit polyclonal anti-TOM20 (1:150, Santa Cruz). After washing with PBS, cells were incubated with Alexa Fluor 568 Goat Anti-Rabbit IgG (1:1000, Life Technologies) for 1 hour at room temperature. Coverslips were mounted on glass slides using ProLong Gold Antifade Reagent (Life Technologies). Where indicated, neutral lipids were stained before mounting with 15 min. incubation with BODIPY 493/503 (2 μ g/ml, Life Technologies). Each transfection was replicated independently five times. Images were acquired with a 60X objective using a confocal spinning-disk microscope (Andromeda iMIC system; TILL Photonics).

For MyHC-2A immunostaining, transfected TA muscles were included in OCT medium and sectioned in 10 μ m slices. TA muscle slices were washed 3 times in PBS. Without any kind of fixation, slices were incubated at 37°C for 1 hour in Mouse on Mouse (MOM) Blocking reagent (Vector Laboratories) (1 drop in 1.25 mL of PBS). After 3 washes in PBS, slices were incubated at 4°C O/N with primary antibodies in 0.5% BSA (in PBS): mouse monoclonal anti-myosin 2A (SC-71 from DSHB, dilution 1:100) and rabbit polyclonal anti-dystrophin (ab15277 from Abcam, dilution 1:100, for the membrane staining). After 3 washes in PBS, slices were incubated at 37°C for 1 hour with the secondary antibody: for myosin 2A, Alexa Fluor 488 IgG1 (Jackson ImmunoResearch, anti-mouse, dilution 1:150); for dystrophin, Alexa Fluor 647 conjugate (Jackson ImmunoResearch, anti-rabbit, dilution 1:100). Slices were washed 3 times with PBS and the slide was mounted with Elvanol mounting medium (Waterborne INC). Fluorescent images were acquired with fluorescence microscope (Cytell, GE Healthcare).

Muscle cryosection staining

Succinate dehydrogenase stain was performed incubating fresh muscle cryosections derived from *gastrocnemius* for 30 min. as described in Blanco et al. (1988). Periodic acid-schiff (PAS) staining was performed on cryosections of *tibialis anterior* following the instructions of PAS staining system (Sigma-Aldrich). Images were acquired with a 10X objective using DMR Leica microscope. Bodipy staining was performed incubating cryosections of *tibialis anterior* with BODIPY 493/503 (2 μ g/ml, Life Technologies) for 20 min. Images were acquired with a 60X objective using Zeiss LM700 Confocal.

Electron microscopy

Samples were fixed with 2.5% glutaraldehyde in 0.1 M sodium cacodylate buffer pH 7.4 for 1 hour at 4°C, post-fixed with 1% osmium tetroxide and 1% in 0.1 M sodium cacodylate buffer for 2 hours at 4°C. After three water washes, samples were dehydrated in a graded ethanol series and embedded in an epoxy resin (Sigma-Aldrich). Ultrathin sections (60–70 nm) were obtained with an Ultratome V (LKB) ultramicrotome, counterstained with uranyl acetate and lead citrate and viewed with a Tecnai G2 (FEI) transmission electron microscope operating at 100 kV. Images were captured with a Veleta (Olympus Soft Imaging System) digital camera.

Western blot

C2C12 cells overexpressing miR27a-3p or -142-3p (myotubes at 7 days of differentiation) were washed with Phosphate Buffer Saline (PBS) and then lysed using a non-reducing buffer containing 10% (v/v) glycerol, 2.3% (v/v) SDS, 62.5 mM Tris/HCl (pH 6.8), and phosphatase and protease inhibitor cocktails (PhosSTOP and cOmplete tables mini – Roche). Samples were centrifuged at 16,000 × g (10 min., 4°C) to remove cell debris. Protein quantification was performed using the Pierce BCA protein assay kit (Thermo Scientific) according to manufacturer's instruction. Myotube lysates were then adjusted to an equal protein concentration using reducing (50 mM dithiothreitol) Laemmli sample buffer and boiled for at least 5 min. Proteins (20 µg) were separated by using the NuPAGE 4%–12% Bis-Tris precast gels (Life Technologies) and then electroblotted onto polyvinylidene difluoride membranes (0.45 µm, Amersham Pharmacia Biotech). PVDF membranes were incubated (1h, room temperature) with a blocking solution [Tris-buffered saline added with 0.1% (w/v) Tween-20 (TBS-T) with 5% (w/v) instant non-fat dry milk (First Street)] followed by incubation with the primary antibody (overnight, 4°C). After three washes (5 min. each in TBS-T), membranes were incubated (1 hour, room temperature) with a horseradish peroxidase-conjugated anti-rabbit-IgG secondary antibody. After three washes (5 min. each in TBS-T), immunoreactive bands were visualized and digitalized with the Alliance Mini HD9 UVITEC imaging system (Eppendorf), using the SuperSignal West Pico Chemiluminescent Substrate (Thermo Scientific). To verify equal loading and transfer, PVDF membranes were stained with Coomassie brilliant Blue (0.1% Brilliant Blue R (Sigma), 50% methanol, 7% acetic acid).

Measurement of oxygen consumption

Oxygen consumption rate (OCR) was measured with the XF24 Extracellular Flux Analyzer (Seahorse Bioscience). C2C12 transfected myoblasts were seeded in XF24 cell culture microplates at 6×10^3 cells/well in 0.2 mL of DMEM containing 25mM glucose and incubated at 37°C in 5% CO₂. Experiments were carried out on confluent monolayers after 72 hours. OCR in 25 mM glucose DMEM was initiated by replacing the growth medium with serum-free DMEM glucose. OCR driven by lipid oxidation was initiated by replacing the growth medium with substrate-limited medium (DMEM with 0.5 mM Glucose, 1 mM glutamine, 0.5 mM carnitine and 1% FBS) 9 hours before the experiment. The medium was replaced with the FA oxidation (FAO) medium (2.5 mM Glucose, 0.5 mM carnitine, 111 mM NaCl, 4.7 mM KCl, 1.25 mM CaCl₂, 2 mM MgSO₄, 1.2 mM NaH₂PO₄, and 5 mM HEPES) 45 min. prior the assay. OCR driven by lipid oxidation was determined by inhibition of the mitochondrial FA importer CPT-I using 40 µM etomoxir added 15 min. before the experiment. Just prior to starting the assay XF Palmitate-BSA FAO substrate (Seahorse Bioscience) was added to the wells. A titration with FCCP was performed for each transfection in order to determine the optimal FCCP concentration (i.e., the concentration that stimulates respiration maximally), which was found to be 0.4-0.6-1 µM for scramble, 0.4-0.6-1 µM for miR-27a, 0.4-0.6-1 µM for miR-142. After OCR baseline was established, a solution containing oligomycin (in 25mM glucose experiment), FCCP, rotenone or antimycin A were sequentially added to each well to reach final concentrations of 1 µg/ml oligomycin, FCCP as stated above, and 1 µM for rotenone and antimycin A. Data are expressed as pmol of O₂ per min. per plated cells. At the end of each experiment, the medium was removed from each well and the total protein content per well was quantified. miRNA transfections were independently replicated at least three times, and for each one five technical replicates were measured.

Lipidomic analysis

Lipids were extracted from transfected cells using a solution 2:1 chloroform:methanol 0.005% BHT. The chloroformic extracts were taken, dried using a rotary evaporator, and dissolved in 150 µL HPLC-grade methanol (Sigma-Aldrich). MS measurements were carried out in both positive and negative ion mode, using a Bruker Esquire-LC quadrupole Ion-Trap mass spectrometer equipped with an electrospray source (Bruker Optik GmbH, Ettlingen, Germany). The spectrometer was coupled to an HPLC (Hewlett–Packard Model 1100 Series) to chromatographically resolve the analytes prior to their mass detection. The chromatographic separation was obtained using a Zorbax Eclipse XDB-C18 column (150 × 4.6 mm I.D., particle size: 3.5 µm; Agilent Technologies). The mobile phase consisted of solvent A, 70:30 methanol:water with 12 mM ammonium acetate, and solvent B, 100% methanol with 12 mM ammonium acetate. The elution program started from 35% B, reached 100% B in 40 min, and kept this composition for 50 min., at the steady flow rate of 0.8 mL/min. For the mass detection, the instrumental parameters were the following: scan range 100–1200 m/z with a frequency of 13000 m/z s⁻¹, nitrogen pressure of 35 psi, temperature of 300°C, and high voltage capillary of either 4000 V (positive ionization mode) or -4000 V (negative mode). The injection volume was 10 µL.

Luciferase assay

Myoblasts were transfected with miRNA mimics and 100 pg/µL of pmirGLO Dual-Luciferase miRNA Target Expression Vector (Promega) containing the target sequence or a control sequence (primers for cloning are listed in Table S4). Assays were performed using the Dual-Luciferase Reporter Assay (Promega), measuring firefly and renilla luciferase activities with Turner Designs TD-20/20 Luminometer (DLReady). miRNA transfections were independently replicated at least three times.

Glycogen assay

Glycogen content in transfected cells was measured using the Glycogen assay colorimetric kit (Abcam) following the manufacturer's instructions. Results derive from the sum of six independent experiments.

Flow cytometry

Transfected C2C12 myoblasts were permeabilized and stained with BODIPY 493/503 (2 µg/ml, Life Technologies) for 15 min. After two PBS washes, cells were transferred in FACS conical tubes and flow cytometry was performed using a BD FACSCalibur platform (Becton Dickinson). Percentage of positive cells was calculated using mock-transfected C2C12 as a negative control. Results derive from the sum of six independent experiments.

QUANTIFICATION AND STATISTICAL ANALYSIS

Microarray data analysis

Data pre-processing

Probes features were extracted using the Feature Extraction Software v. 10.7.3.1 with GE_1_Sep09 protocol (Agilent Technologies). Intra-array normalizations were directly performed by the Feature Extraction Software. Quantile inter-arrays normalization was performed using the Expander software (Sharan et al., 2003). Data were Log_2 transformed and not available (NA) value was assigned if Found and/or Well Above Background flags were not positive. Expression values of probes with the same sequence were mediated. In myofiber microarray experiments, 10 myofibers per each of 6 myofiber types (classified by MyHC protein expression, total: 60 microarrays) were analyzed. Only probes with at least 8 of 10 available values in at least one myofiber type were taken into consideration for the further analyses. In cells microarray experiments, 6 independent replicates for miRNA mimic transfected cells, and 4 independent replicates for cells transfected with a scrambled sequence (used as control) were analyzed. Only probes with at least 75% of available values in at least one condition were taken into consideration for the further analyses.

Statistical analyses of microarray data

Microarray data were analyzed using the MultiExperiment Viewer (MeV, Ver. 4.8), a tool of TM4 Microarray Software Suite (Saeed et al., 2003). To identify the DE probes among myofibers, we performed one-way analysis of variance (ANOVA). Each sample was assigned at one of the 6 groups identified by the MyHC protein classification. Probes with an adjusted Bonferroni P value (based on 1,000 permutations) lower than 0.01 were considered as DE. In addition, to improve the number of genes DE, probes not recognized by the statistical test and exclusively expressed in 1 or 2 clusters were manually added to the list. Samples (myofibers) were hierarchically clustered using the Pearson's correlation distance and average linkage method. DE probes were grouped in 8 different clusters by K-means clustering, on the basis of their expression. Intensity values of the probes of the same cluster and of the same transcriptional class were mediated and differences among classes were considered statistically and biologically significant if the adjusted P value generated by ANOVA was < 0.01 (calculated with GraphPad Prism software) and the difference of means > 1 .

To identify the DE probes in transfected cells, we performed Significance Analysis of Microarrays (SAM), a non-parametric statistical test based on a permutation approach specifically implemented for microarray data, imposing a threshold level of False Discovery Rate of 0.05% (Tusher et al., 2001).

Gene ontology

DE genes were categorized in gene ontology (GO) classes using the Functional Annotation Clustering method, a bioinformatic tool of the DAVID database (Huang et al., 2009). Only GO terms with an enrichment score greater than 1.3 and with P value less than 0.05 were considered.

Analysis of discriminant genes

The list of the best marker genes among transcriptional myofiber classes was obtained applying Prediction Analysis of Microarray (PAM) algorithm (Tibshirani et al., 2002). PAM utilizes the shrinkage nearest centroid method that does automatic gene selection. Missing values are imputed using a K-nearest neighbor average in gene space ($K = 10$).

Sequencing data processing

Raw reads were trimmed and cleaned-up using an in-house developed program that: a) identifies the barcodes of the different myofiber types; b) removes adapters; c) keeps only the reads longer than 18 nucleotides. The expression of miRNAs was quantized using miRDeep software (Friedländer et al., 2008). The processed reads were mapped to the known mouse miRNA precursors from miRBase database (Ver. 19) using the mapper module of miRDeep with default values. Basically, in this process equal reads are counted and collapse. Reads that mapped more than 5 times are automatically excluded. Quantize module was used to normalize read counts of mature miRNAs.

Analysis of miRNA families

Enriched miRNA families analysis was performed on miRNAs obtained from NGS of myofibers using miR Family TargetScan database (Ver. 6.2). Only families with a P value (Benjamini-Hochberg adjusted) lower than 0.05 and at least 2 identified miRNAs were considered statistically significant.

Construction of mRNA-miRNA network

miRNA targets were identified using miRSVR (August 2010 release) and TargetScan (Ver. 6.2) prediction algorithms. Pearson's correlation between mRNA (from microarray) and miRNA (from sequencing) expression data was performed with Excel (Microsoft Office). Only interactions with a correlation coefficient < -0.3 were considered anti-correlated. Networks were generated and analyzed using Cytoscape software (Ver. 3.2, (Shannon et al., 2003)).

Statistical analysis

All the experiments shown in the manuscript were performed at least in triplicate (exact values of n for each experiment are indicated in the figure legends) and statistical analyses were performed with GraphPad Prism software.

qRT-PCR data analysis

The threshold cycle (Ct) was defined as the fractional cycle number at which the fluorescence exceeds the fixed threshold of 0.2. To evaluate differences in mRNA expression, a relative quantification method was chosen where the expression of the mRNA target is standardized by the Txn1 endogenous mRNA, whose level remains essentially constant among different samples (Chemello et al., 2011). To evaluate differences in miRNA expression, relative quantification was performed using the ExpressionSuite Software (Ver. 1.0, Thermo Fisher Scientific) and U6 as endogenous standard miRNA. Pearson's correlation with sequencing data was performed with Excel.

Image analysis

For mitochondrial image analysis, Z stacks images of ten randomly chosen fields for each coverslip were acquired and stored for subsequent analysis. Quantification of the fragmentation index f of mitochondrial networks, defined as the sum of relative fragment areas that individually constitute less than 20% of the total mitochondrial area, was performed using MitoLoc software (Vowinckel et al., 2015). All the images were processed using ImageJ software.

Western blot analysis

For densitometric western blot analysis, the intensity of each immunoreactive band was normalized to the optical density of the corresponding Coomassie blue-stained lane as in Gilda and Gomes (2013), Li and Shen (2013), Moritz (2017), Rivero-Gutiérrez et al. (2014), and Welinder and Ekblad (2011).

Lipidomic analysis

The lipid quantitation was performed by integration of the extracted ion chromatograms (XIC), achieved through the proprietary software Bruker Daltonics esquireLC 4.5. Overall, the following lipid classes were detected: lyso-phosphatidylcholines (LysoPC), sphingomyelins (SM), phosphatidylcholines (PC), phosphatidylethanolamines (PE), phosphatidylinositols (PI), diglycerides (DAG), triglycerides (TAG), cholesteryl-esters (CE) and cholesterol. In order to compare the results across samples, the signal areas were normalized to the number of cells relative to each sample, which were therefore used as a reference for the quantitation.

DATA AND SOFTWARE AVAILABILITY

The accession number for the raw microarray data reported in this paper is NCBI GEO: GSE98328. The accession numbers for the miRNA-Seq of isolated myofibers are NCBI SRA: SRX2768351 (fast myofibers), SRX2768352 (intermediate myofibers), and SRX2768353 (slow myofibers).